EXPERIMENTAL INVESTIGATION OF AN AIRFOIL WITH CO-FLOW JET FLOW CONTROL

By

ADAM JOSEPH WELLS

A THESIS PRESENTED TO THE GRADUATE SCHOOL
OF THE UNIVERSITY OF FLORIDA IN PARTIAL FULFILLMENT
OF THE REQUIREMENTS FOR THE DEGREE OF
MASTER OF SCIENCE

UNIVERSITY OF FLORIDA

2005

ACKNOWLEDGMENTS

The author expresses special thanks to the supervisory committee chairman, Dr. Bruce F. Carroll, for his continued guidance, encouragement and devotion. Appreciation is also due to Dr. Ge-Cheng Zha, whose passion for the co-flow airfoil is contagious. Gratitude is also addressed to the other supervisory committee members, Dr. Lou Cattafesta and Dr. William Lear Jr., for their support. The author also wishes to acknowledge all family and friends that helped make this possible.

TABLE OF CONTENTS

LIST OF TABLES

Table page

LIST OF FIGURES

Abstract of Thesis Presented to the Graduate School
of the University of Florida in Partial Fulfillment of the
Requirements for the Degree of Master of Science

EXPERIMENTAL INVESTIGATION OF AN AIRFOIL
WITH CO-FLOW JET FLOW CONTROL

By

Adam Joseph Wells

August 2005

Chair: Bruce F. Carroll
Major Department: Mechanical and Aerospace Engineering

This thesis describes the effort to experimentally verify the high performance characteristics of the co-flow jet (CFJ) airfoil. The CFJ utilizes tangentially injected air at the leading edge and tangentially removed air at the trailing edge to increase lift and stall margin and also decrease drag. The mass flow rates of the injection and suction are equal, so there is a zero net mass flow rate. The existing MAE subsonic Aerolab wind tunnel with a one-foot by one-foot test section was modified to accommodate the injection and suction needed for the CFJ airfoils. The compressor and vacuum systems were reconfigured so the mass flow rate of air could be measured and controlled. The sting balance used to hold the airfoil in the test section and gather lift and drag information was also modified from a previous design.

Two airfoils were tested at the University of Florida. One airfoil had an injection slot size of 0.65% chord length (chord length was six inches) and the other had an injection slot size twice as large or 1.31% chord length. Both airfoils had a suction slot

size of 1.96% chord length. The smaller injection slot size performed superior for increased lift and stall margin, whereas the larger injection slot size performed superior for decreased drag. The smaller injection slot airfoil had an increase in maximum lift of 113% to 220% and an increase in stall margin of 100% to 132% when compared to the baseline airfoil. When the mass flow rate was run at high levels, negative drag (i.e., thrust) was measured for both airfoils.

Particle image velocimetry (PIV) was used to quantify the flow field over the suction surface of the CFJ airfoils. The stagnation point was also studied from the PIV images. Although the movement due to variations in the mass flow rate could be seen, the exact location of the stagnation point could not be seen with the current setup because it lies on the pressure surface of the airfoil. The PIV images also helped in studying the wake of the airfoils. A wake surplus could be seen in the CFJ airfoils, whereas a conventional airfoil would have a wake deficit.

CHAPTER 1
INTRODUCTION

The objective of the wind tunnel experiments described in this thesis is to verify the high performance capabilities of the co-flow jet (CFJ) airfoil. This new flow control technique was suggested by Zha and Paxton [1]. The CFJ uses circulation control to achieve this high performance. More specifically, the CFJ uses leading edge blowing and trailing edge suction. This thesis also presents the effort it took to set up and test the CFJ airfoil. Many modifications were made to existing system to implement the injection and suction needs of the CFJ airfoil.

Flow control offers many benefits to aircraft for both commercial and military uses. The primary advantage of these control techniques is the enhanced lift and suppressed separation. Results of these benefits are shorter take-off and landing distances, increased maneuverability, increased payloads, reduced fuel consumption and reduced weight.

There are a number of flow control techniques that are being used today. These include rotating cylinders at the leading and trailing edge [2], blowing at the leading edge [3,4], blowing at the trailing edge [5-7], pulsating jets [8-10] and multi-element airfoils [11,12].

The CFJ has advantages over the flow control methods mentioned by requiring no moving parts, not requiring a feedback control system and having a net mass flow rate of zero. Moving parts add weight to the aircraft. Feedback control systems add complexity and could also add weight to the aircraft. Blowing air has a direct and adverse effect on the propulsion system if it is taken from the compressor stage of the engine or adds

weight to the aircraft if a compressor system is added. The mentioned control systems are limited by one or more of these constraints.

Another advantage of the CFJ is that it can be implemented on any airfoil shape. It can be used on a thick subsonic airfoil as well as a thin supersonic airfoil. Some of the other flow control techniques need thick leading or trailing edges, which drastically increase the drag force during cruise and limit the number of airfoils to which the technique is applicable.

The CFJ has proven to be effective at increasing lift and stall margin while decreasing drag at the same time [13]. This is accomplished with little penalty to the propulsion system by having a net mass flow rate of zero as mentioned earlier. The mass of air that is injected at the leading edge is equal to the mass of air that is removed at the trailing edge. The pulsed jet or synthetic jet, another zero mass flow rate technique, increases $C_{L\max}$ by about 35% and has little effect on the stall angle for a jet momentum coefficient of 0.022 [9]; the CFJ increases $C_{L\max}$ by 220% and the stall angle by 132% for a jet momentum coefficient of 0.28.

CHAPTER 2
APPARATUS MODIFICATIONS AND ASSEMBLY

This chapter is dedicated to the description of the CFJ airfoil and the modifications made to the existing systems to enable testing of the CFJ airfoil. This section will also include the instrumentation and measurement techniques used in the wind tunnel experiments. An uncertainty analysis on all measured and calculated values is included at the end.

Co-Flow Jet Airfoil Description

The CFJ airfoils used in testing at the University of Florida were a modified NACA 0025. The NACA 0025 airfoil was chosen for its ease of manufacturing and relative thickness. The thickness made it easier to fit all instrumentation and duct work into the airfoil given the size constraints imposed by the one-foot by one-foot wind tunnel test section; however the CFJ concept can be implemented on any airfoil geometry.

The modified NACA 0025 airfoil used in testing had a span of 0.3m and a chord length of 0.1527m. As shown in figure 2-1, the airfoil was modified by recessing the suction surface (upper surface). This recession opened up a slot towards the leading edge of the airfoil (injection slot) and another slot towards the trailing edge (suction slot). The slot towards the leading edge was used to inject air tangentially over the suction surface, while the slot towards the trailing edge was used to remove air tangentially from the suction surface. Two airfoils were manufactured with this modification. The first had a 1mm or 0.65% chord length injection slot height. The second had a 2mm or 1.31% chord length injection slot height. Both airfoils had a 3mm or 1.96% chord length suction slot

height. The airfoils are named by their injection and suction slot sizes according to the convention CFJ4digit-INJ-SUC. So the airfoil with the 1mm injection slot was named CFJ0025-065-196. Similarly, the airfoil with the 2mm injection slot was named CFJ0025-131-196.

The reason the suction slot size was larger than the injection slot is because the density of the air being removed by the suction slot is less than the density of the air being injected. Therefore, to balance the mass flow rates, the suction area has to be larger or the velocity greater. But the velocity is limited because the flow will eventually become choked.

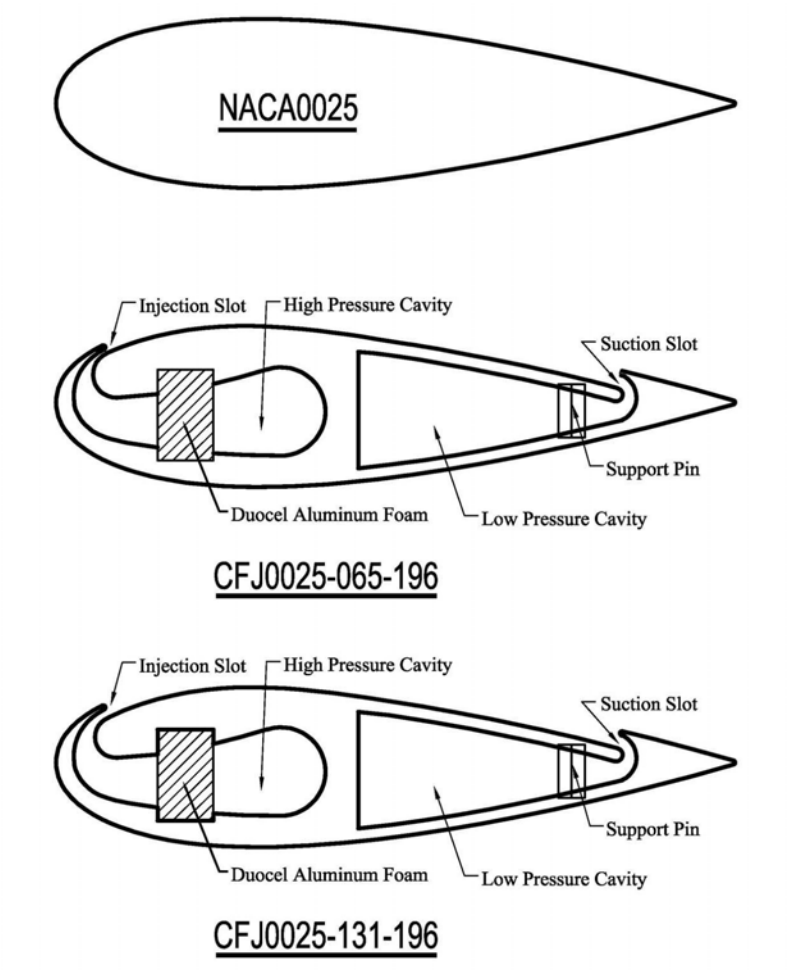

Figure 2-1. 2-D cross section of CFJ airfoils

The location of the injection slot and suction slot are respectively, 7.11% and 83.18% of the chord length from the leading edge. The slots are positioned perpendicular to the suction surface making them parallel to the flow direction.

The support pins shown in figure 2-1 are to reinforce the suction surface of the airfoil because computer simulations indicated the suction surface might deflect in that area. The Duocel aluminum foam is used to create a backpressure in the high-pressure cavity ensuring an even distribution of air across the suction surface.

A filler piece was fabricated to fill the recessed portion of the CFJ0025-131-196. With the recession filled in, the airfoil was a NACA 0025. This was referred to as the baseline airfoil and was used as a comparison for the CFJ airfoils. Figure 2-2 shows how the filler piece fits into the CFJ0025-131-196.

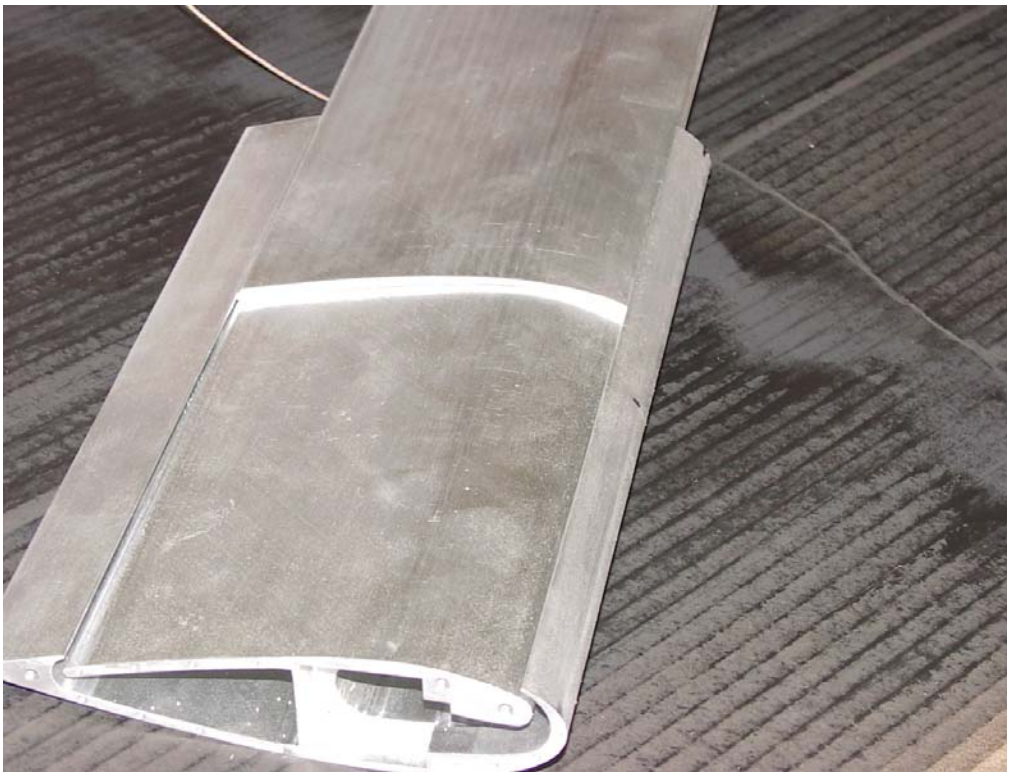

Figure 2-2. How CFJ0025-131-196 turns into NACA 0025

Wind Tunnel Modifications

An open loop Aerolab wind tunnel was used to test the CFJ airfoils. The wind tunnel has a test section that measures 0.305m x 0.305m (12 inches x 12 inches) and is 0.610m (24 inches) long. The tunnel is 4.57m (15 feet) long overall and has an operating speed from 0-65 m/s (0-145 miles per hour). This is made possible by a 10-horse power motor that drives a fan. Figure 2-3 shows a picture of the unmodified Aerolab wind tunnel.

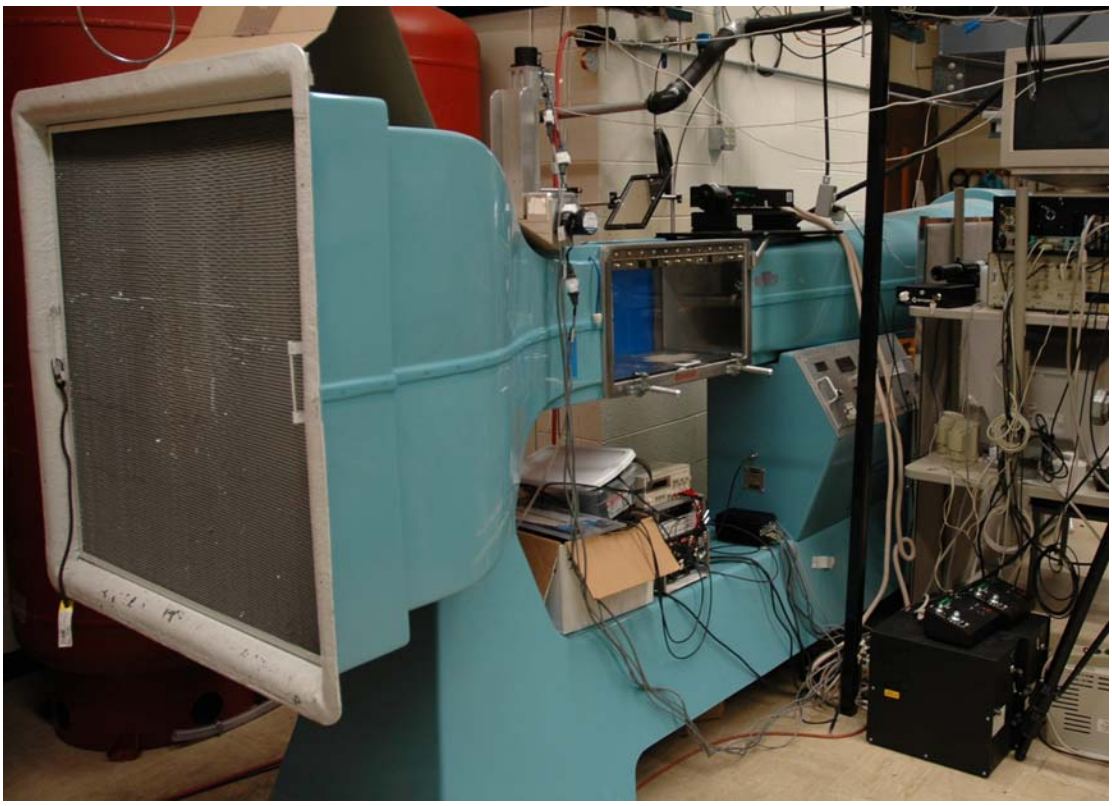

Figure 2-3. Unmodified Aerolab wind tunnel

In order to operate the injection and suction of the CFJ airfoils, many modifications had to be made to the existing Aerolab wind tunnel. The wind tunnel had to be equipped with a system to inject the desired mass flow of air. The tunnel also needed the capability to remove the air from the suction slot of the airfoil. Injecting air through the sting

balance that supports the airfoil in the wind tunnel and building a Plexiglas box on the opposite side overcame these two problems. Figure 2-4 shows the modified Aerolab wind tunnel.

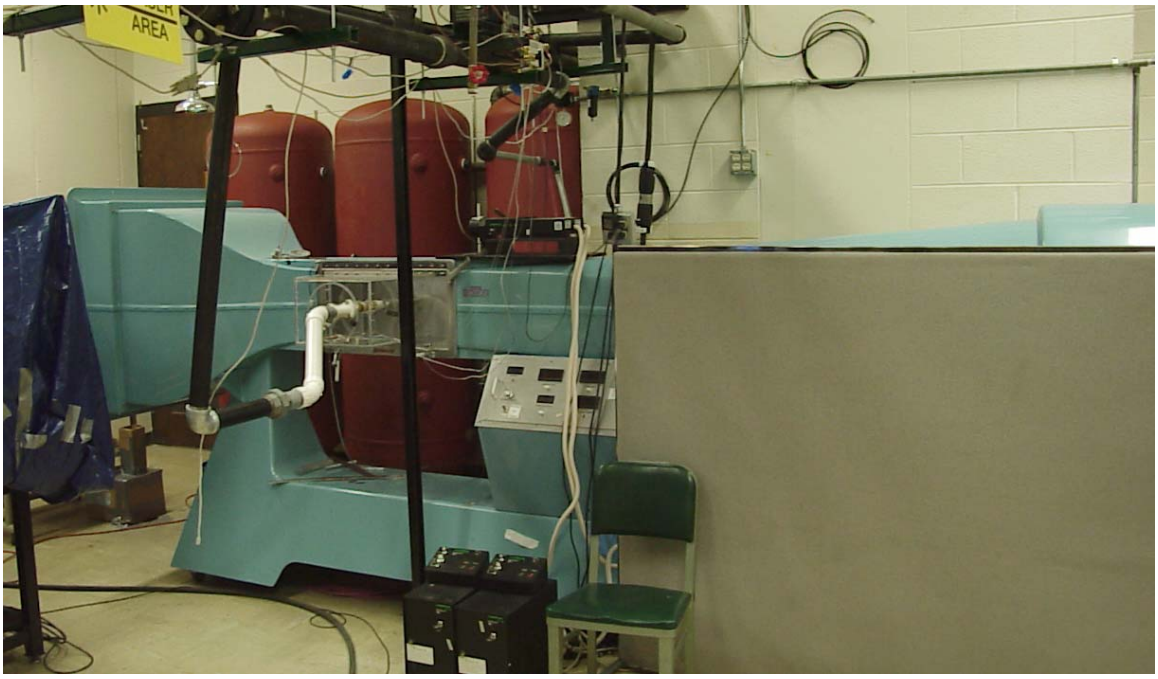

Figure 2-4. Modified Aerolab wind tunnel

An existing sting balance used to measure lift and drag forces was modified for the new wind tunnel needs. The balance is discussed in more detail later in the chapter. The cylinder of the balance, which attaches the airfoil to the rest of the balance, was lengthened so it would completely pass through the mounting components of the balance. With the extension, there was room to attach a pressure hose and clamp (figure 2-5 shows the hose/clamp and cylinder attachment). Compressed air is then forced through the hollow cylinder into the airfoil where it passes through porous aluminum foam and is injected tangentially over the airfoil (the connection between the balance cylinder and the airfoil can be seen in figure 2-6). The foam creates backpressure and ensures uniform distribution of air across the span of the airfoil.

Figure 2-5. Hose/clamp attachment to cylinder and balance mechanism. Airfoil is attached in horizontal position inside tunnel

Figure 2-6. Connection between the balance cylinder and the airfoil

The opposite side of the wind tunnel originally had a flat Plexiglas wall. This was removed in order to accommodate the suction system. A suction manifold was installed on this side of the airfoil (figure 2-7 shows the connection between the suction manifold and the airfoil). The manifold extends beyond the limits of the test section. A Plexiglas box was designed to encompass the manifold. The outside of the box was sealed as to not let air leak into the test section. The inside circular wall of the box was cut out around the manifold and stagnation pressure probe (figure 2-8 shows the circular wall and suction manifold inside of the Plexiglas box). The circular wall allowed enough clearance to accommodate any deflections of the airfoil from the lift and drag forces. If the airfoil deflected into the wall, some forces would be imposed onto the wall; therefore the lift and drag measurements would not be accurate.

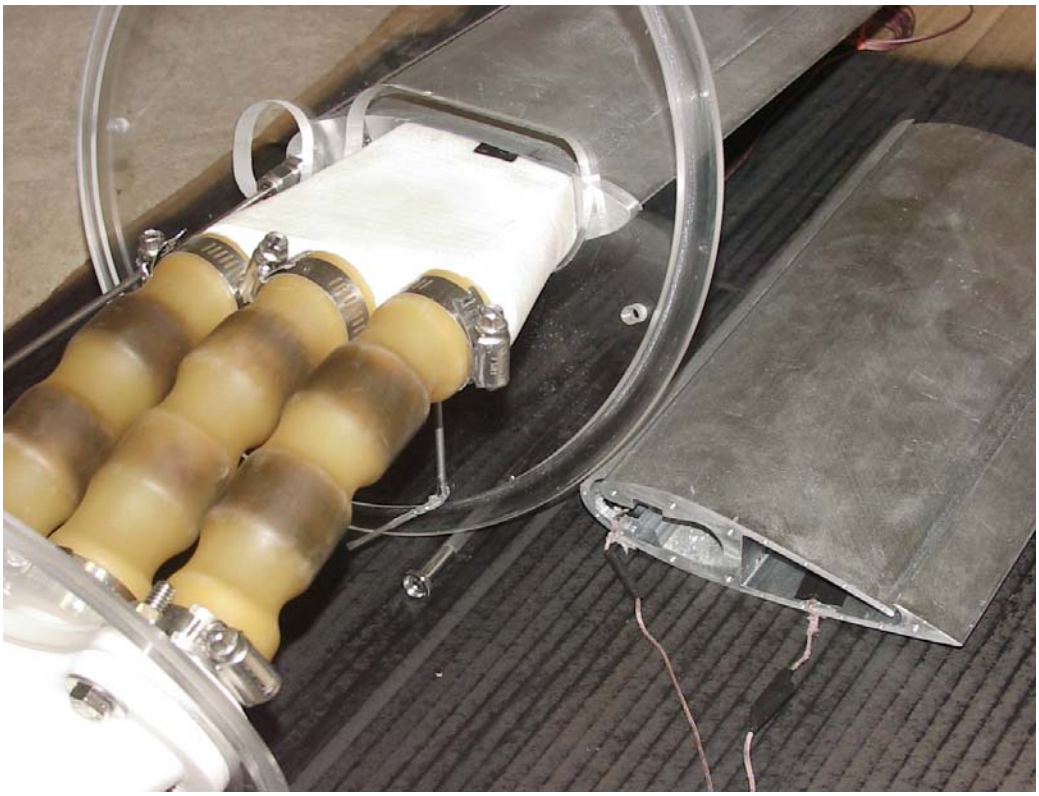

Figure 2-7. Connection between the suction manifold and the airfoil

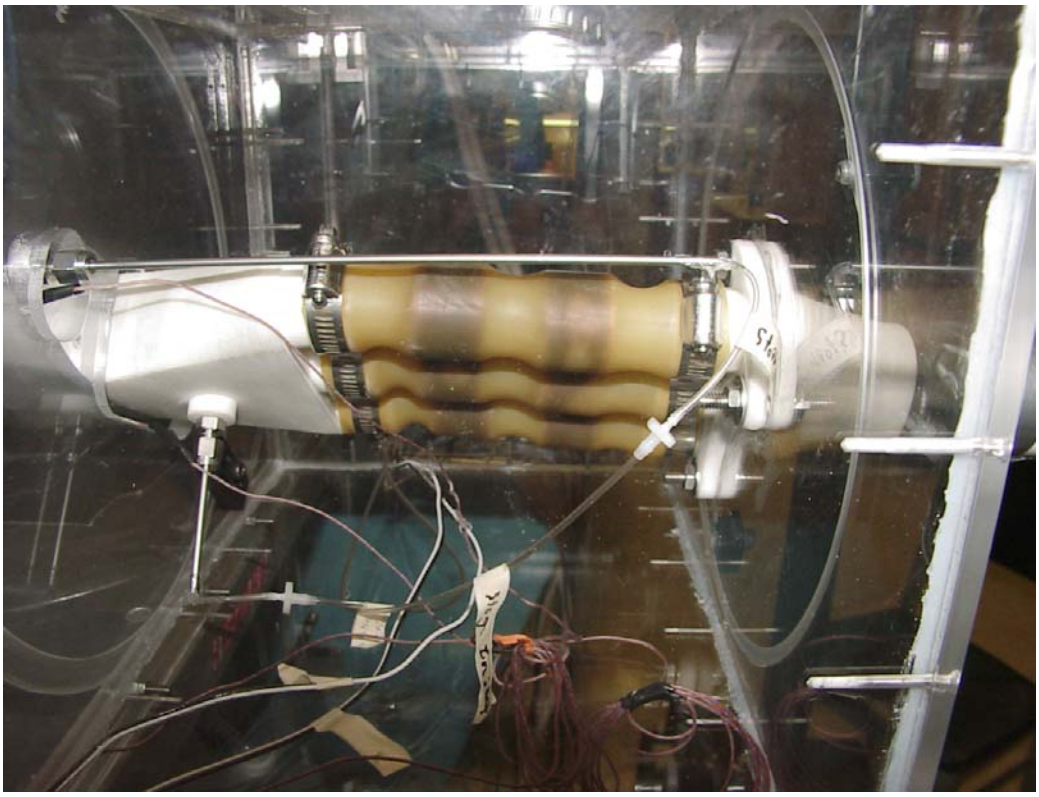

Figure 2-8. Plexiglas box and suction manifold with airfoil located to the left and external suction connection to the right

Mass Flow Rate Controls

The enhanced performance of the CFJ airfoil comes from the air that is injected at the leading edge and removed at the trailing edge; therefore it is critical to control the injection and suction mass flow rates of air. The two mass flow rates were controlled in different manners due to the different systems available at the time of testing.

A compressor supplied the air that was injected at the leading edge. The compressor, located outside of the building, is attached to two reservoir tanks of 3700 gallons volume each. The reservoir tanks are pressured up to 200 psig. The compressor is designed to hold the tanks at this pressure. The amount of air that passes through the injection slot is much less than the capability of the compressor (950 scfm). Therefore the stagnation pressure inside the reservoir tanks is always constant.

From the reservoir tanks, the air flows into the building and passes through two valves before it makes it to the airfoil. The first valve acts to throttle the air to a lower pressure; this is done with a ball valve that is manually cracked open. The valve is usually opened about a quarter of the way but is adjusted depending on the desired mass flow rate. The second valve acts to control the mass flow rate and/or injection stagnation pressure. This valve is a pneumatic control valve that is operated through a computer in an open loop control system. The valve was adjusted to dial in the desired mass flow rate, which was measured with an orifice plate.

The suction mass flow rate was designed entirely different. The facilities at UF did not include a vacuum pump designed to displace a large volume of air. Two vacuum pumps were available but they were designed to obtain a low pressure and hold it; to solve the problem, vacuum tanks were added onto the existing system. The total volume of the tanks would have to be large enough for the suction to last at least 15 seconds at the highest mass flow rate. UF already had around 480 gallons of vacuum tank space between three different tanks. An additional three tanks of 240 gallons each were added, bringing the total vacuum tank space to around 1200 gallons.

The addition of the tanks solved the vacuum pump deficiency, however the mass flow rate still needed to be controlled. The idea of choking the pipe prior to the vacuum tanks was chosen as the solution. A two-valve system was designed to accomplish this. The first valve was to open and close the pipe. This valve can be thought of as an on/off switch and was always in the fully open or fully closed position. The second valve, located closer to the vacuum tanks, was used to control the mass flow rate. This valve was a gate valve. A gate valve was chosen because of the greater accuracy in adjusting

the effective flow area. Since the upstream stagnation pressure is constant, the inside area of the pipe is the only variable that effects the mass flow rate.

The vacuum system must always be used in a choked condition to have a constant mass flow rate. The requirement for a choked system is the ratio of static pressure downstream of the valve to the stagnation pressure upstream of the valve to be less than .5283. So the system could only run until this requirement was no longer met.

The injection and the suction mass flow rates were measured using orifice plates. Equation 2-1 relates the mass flow rate to the differential pressure across the orifice plate and the upstream density. Table 2-1 gives values for all constants in equation 2-1.

$$q_m = \frac{CE\varepsilon\pi d^2\sqrt{2\rho_1\Delta p}}{4} \qquad \text{Eqn 2-1}$$

where,

q_m	Mass flow rate
C	Discharge coefficient
$E = \frac{1}{\sqrt{1-\beta^4}}$	Velocity approach factor
D	Inner pipe diameter
β	Ratio of orifice diameter to inner pipe diameter
ε	Gas expansion factor
d	Orifice diameter
ρ_1	Upstream density
Δp	Differential pressure across orifice plate

Table 2-1. Orifice plate 1494 coefficients

Coefficient	Injection Side	Suction Side
C	0.6079	0.6117
E	1.048	1.111
ε	0.9949	0.9659
d	1.682 in	2.026 in

The differential pressure was measured from the flanges housing the orifice plate. The upstream density was found by measuring the upstream temperature and pressure.

Once the temperature, T, and pressure, P, were found, the density was obtained from the ideal gas law given in equation 2-2 with R being the gas constant for air.

$$\rho = \frac{P}{RT} \qquad \text{Eqn 2-2}$$

A 0-50 inH_2O differential pressure transducer was used to measure the differential pressure across the orifice plate. Only one 0-50 inH_2O differential pressure transducer was available at the time of testing. Therefore it was impossible to measure two different mass flow rates simultaneously. A manual switch was implemented to go back and forth from measuring the injection and suction mass flow rates.

Balance Modifications

The balance used to measure lift and drag forces in the Aerolab wind tunnel was modified from a balance previously designed at the University of Florida. The main features of the balance will be described here. For an in-depth description of the balance and the calibration of the balance, the author refers the reader to reference 14.

The balance was designed in such a way that when the angle of attack is changed, the airfoil does not cause a severe blockage in the wind tunnel. Although at extremely high angle of attacks, some blockage effects were unavoidable. The extent of the blockage was not taken into account. The free stream velocity was calculated from the dynamic pressure of the test section upstream the airfoil.

The balance was designed in such a way that the airfoil would not deflect more than 1mm on the free end. This was to ensure the strain on the cylinder supporting the airfoil was within the limits of the strain gauges (where lift and drag measurements are taken). In experiments, this 1mm deflection was exceeded. The deflection of the CFJ airfoil is estimated to be 3mm; however exceeding this design parameter is not a concern.

The deflection is still small enough to allow for a small angle approximation for lift and drag. That is, lift is still assumed in the normal direction to the floor of the wind tunnel test section and drag is still assumed in the direction of the free stream. More importantly, the limitations of the strain gauges were not exceeded.

The balance was designed in such a way that the wires from the strain gauges could transverse through the side of the wind tunnel while the wind tunnel itself kept an airtight seal. The wind tunnel velocity is calculated from the dynamic pressure of the tunnel, so any air leaks into the tunnel could falsify the velocity reading. If there were airflow into the tunnel, the aerodynamic performance of the test airfoil would also be jeopardized.

The basic design of the balance was kept. The same canister, cullet and tunnel wall were all used. The airfoil is connected to the cylinder in the same manner, although, a new endplate and cylinder was designed to meet the air injection needs.

The original cylinder was designed to fit flat on the endplate. A gasket was sandwiched between the two to form an airtight seal. A new cylinder and endplate were fabricated so the cylinder would travel through the endplate. The new cylinder was lengthened so it would extend 10 inches past the endplate; this was necessary to inject compressed air into the airfoil. Compressed air was injected into the cylinder from a hose that was clamped on the free end outside the balance.

The hole in the middle of the endplate was made large enough to accommodate the width of the cylinder. An o-ring was seated into a small recess in the endplate hole. The o-ring sealed the balance and made the side of the wind tunnel airtight.

Calibration of Airfoil

The calibration of the airfoil was modified from a previous calibration procedure. The calibration procedure calibrates for lift, drag and pitching moment. However, it was

later found the pitching moment was unreliable due to the latex tubes attached at the suction side of the airfoil. The calibration procedure is outlined here. A detailed calibration procedure can be found in appendix A.

The hollow cylinder from the balance was fixed in position at an appropriate angle. An appropriate angle corresponds to an angle inside the airfoil's angle of attack margin. The CFJ was tested from -10 deg to 45 deg, so an appropriate angle would fall anywhere between these two limits.

A metal calibration bar was then attached to the end of the cylinder that holds the airfoil. The angle of the calibration bar was entered into a Labview program. The calibration bar has a hole in it (a know distance from the cylinder) from which a known weight was hung. The program converts the weight to the appropriate load measurement (normal force, axial force and pitching moment). The voltage from the strain gauge's Wheatstone bridge is recorded. More weight is then added. This process is repeated until the weight has exceeded the maximum aerodynamic force expected.

The whole process was then repeated for different angle of attacks. The entire calibration process was then performed again to check for repeatability in the calibration curves. The variations in calibration curves are due to imperfection in the placement of the strain gauges on the metal cylinder and bonding of the strain gauges to the metal cylinder. Other imperfections include the solder joints and minute differences in the strain gauges themselves.

Once a number of calibration curves were gathered, the slopes were averaged to come up with a calibration that was applicable to all angle of attacks. Figures 2-9 and 2-10 are samples of calibration curves for the normal force and axial force respectively.

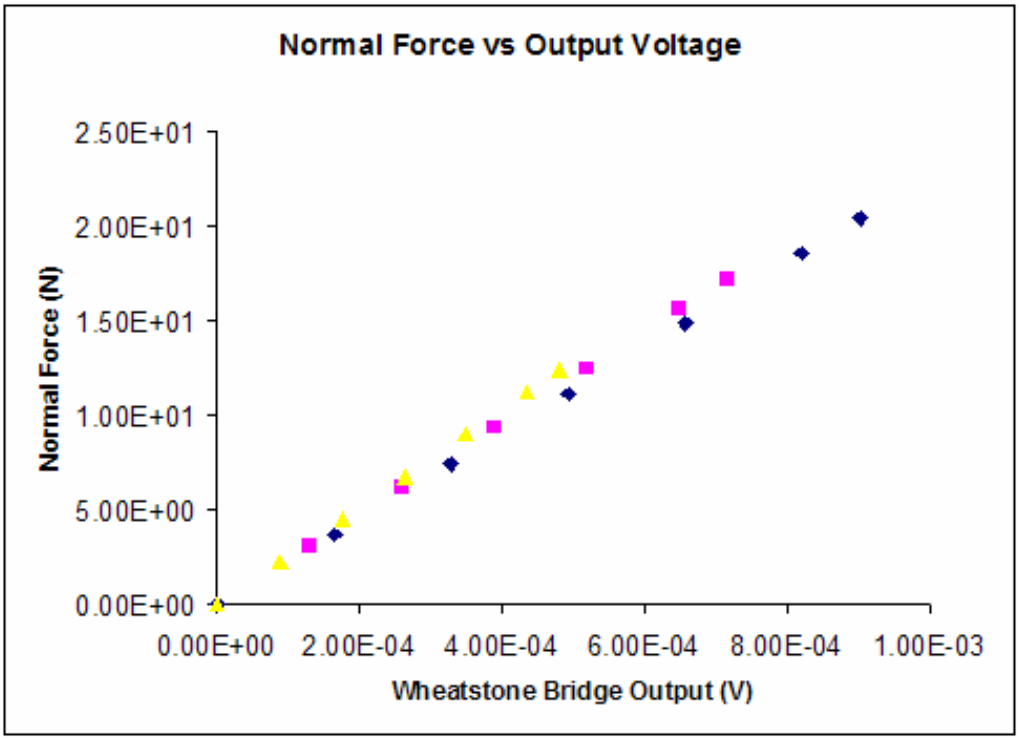

Figure 2-9. Normal force calibration curves

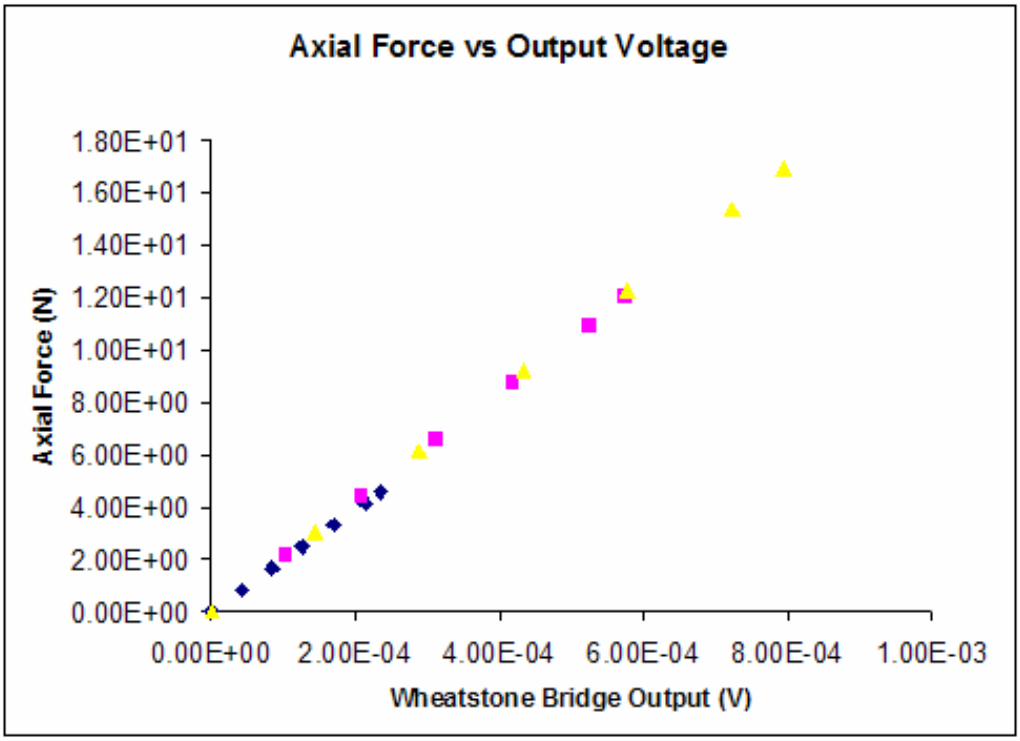

Figure 2-10. Axial force calibration curves

After the initial calibration, the airfoil needs to be placed into the wind tunnel so the effect of the latex tubes can be accounted for. The airfoil is first placed in the wind tunnel with the suction surface facing down so the load to be added acts in the positive lift direction. Known weights are then placed on the center span of the airfoil (the program converts normal and axial forces to lift and drag forces). The known weight is recorded along with the indicated force from the Labview VI used in the testing. Again, this process is repeated, adding more weight until the load exceeds the expected lift force. A calibration factor is then found from the slope of the curve that plotted the known weight verse the force read from the Labview VI used in testing. A similar process is performed for the drag direction. Figures 2-11 and 2-12 are samples of the correction curves; the first is for lift and the second is for drag.

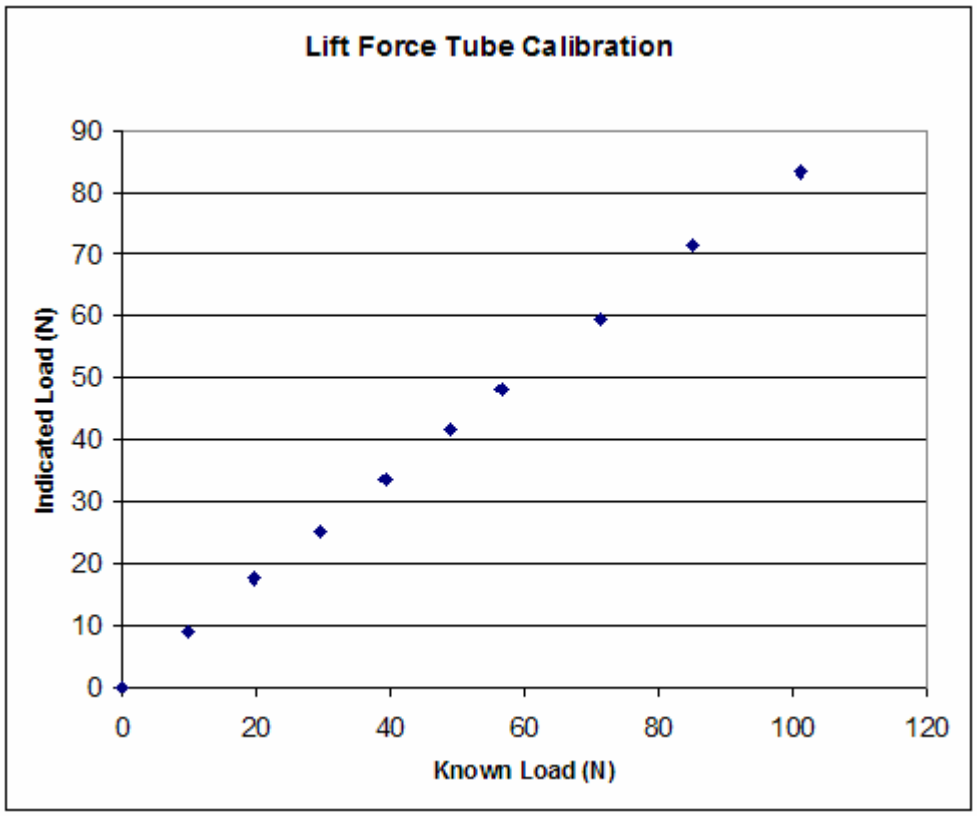

Figure 2-11. Lift correction curve

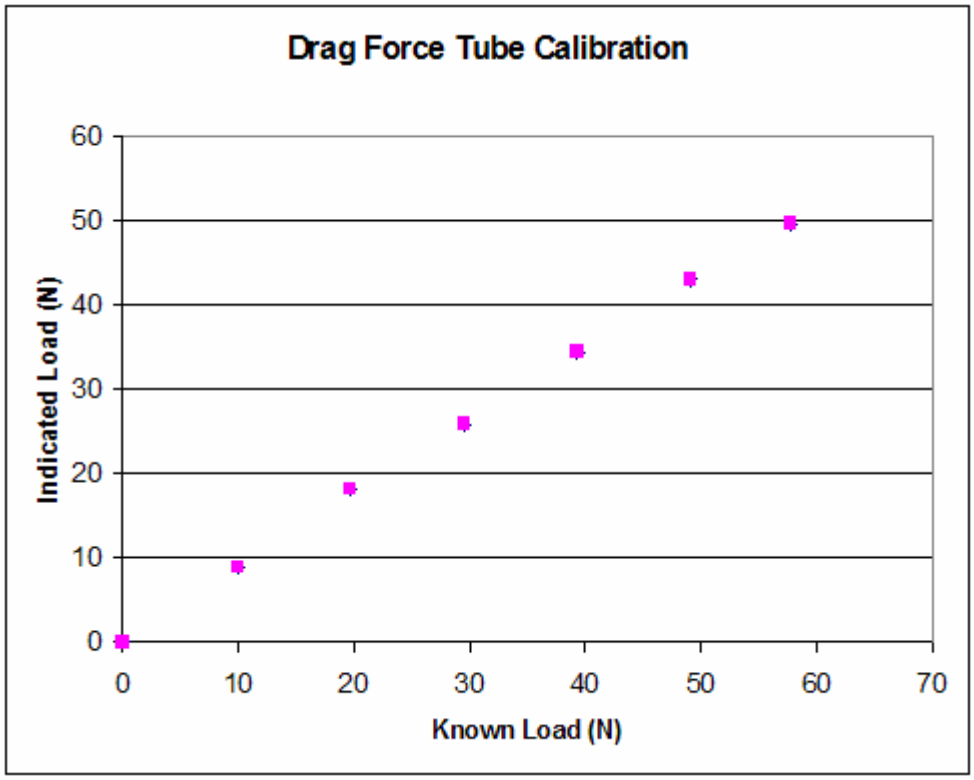

Figure 2-12. Drag correction curve

It was found the latex tubes have a small impact on the lift and drag. The impact of the latex tubes was linear in both the lift and drag directions and therefore easily corrected. However, the impact of the latex tubes was significant in the pitching moment and therefore the measurement was considered unreliable. The reason for this is the pitching moment is greatly influenced by the deflection in both the lift and drag direction. After the airfoil is calibrated inside the test section of the wind tunnel, the airfoil is righted and testing proceeds.

Instrumentation and Measurements

This section describes the measurements took during wind tunnel testing and the instrumentation used to take the measurements. A detailed list of all instrumentation can be found in appendix B.

The wind tunnel velocity was calculated from the dynamic pressure, $\frac{1}{2}\rho v^2$, of the test section. A 0-15 inH_2O differential pressure transducer was used to measure the dynamic pressure by measuring the difference between the static pressure in the test section upstream of the airfoil and the stagnation pressure in the room. The velocity was multiplied by a correction factor, found from previous experiments, to account for the losses in stagnation pressure that occur in the tunnel inlet.

The mass flow rate was calculated using equation 2-1. All the values in this equation are constants except the upstream density and differential pressure across the orifice plate. As described earlier in the chapter, the density was found by measuring the upstream temperature and pressure and the differential pressure was measured directly by a 0-50 inH_2O differential pressure transducer.

The injection velocity was also calculated and recorded in wind tunnel testing. To calculate this velocity, the ratio of the local duct area to the sonic throat area must be found. This relation can be seen in equation 2-3.

$$\frac{A}{A^*} = \frac{KP_0 A_{jet}}{q_m \sqrt{T_0}} \qquad \text{Eqn 2-3}$$

where,

K	$0.040416\ \frac{s\sqrt{K}}{m}$
P_0	Total pressure in injection slot
A_{jet}	Injection slot area
q_m	Mass flow rate
T_0	Total temp injection slot

Second the area-Mach number relation must be found; this was done by a linear interpolation of A/A* and Mach number. The interpolation was incremented from Mach

number 0.1 to 1 at intervals of 0.02. Once the Mach number was found, the velocity was calculated using equation 2-4.

$$v_{jet} = M\sqrt{\gamma RT} \qquad \text{Eqn 2-4}$$

where,

v_{jet} Injection velocity
M Mach number
γ Specific heat ratio
R Gas constant
T Static temperature

The jet momentum coefficient was another item calculated and recorded by the program. The jet momentum coefficient is defined in equation 2-5.

$$C_{\mu} = \frac{q_m v_{jet}}{0.5\rho_{\infty} v^2{}_{\infty} S} \qquad \text{Eqn 2-5}$$

where,

C_{μ} Jet momentum coefficient
q_m Mass flow rate
ρ_{∞} Free stream density
v_{∞} Free stream velocity
S Airfoil surface area

The flow was assumed incompressible, so the free stream density was equal to the ambient density and the free stream velocity was equal to the wind tunnel velocity.

The lift and drag forces were measured with strain gauges located on the hollow cylinder of the sting balance. There were a total of 12 strain gauges on the cylinder. Four were for pitching moment, four for drag and four for lift. However, the pitching moment measurements were considered unreliable due to the latex tubes. Out of the four strain gauges for drag, two were placed on one side of the cylinder and two on the side directly opposite allowing for a full Wheatstone bridge configuration to be used.

Therefore, two gauges will be in compression while the other two will be in tension. The same is true of the strain gauges used to measure lift. The voltage across the lift and drag bridges were measured with a data acquisition/switch unit.

A Labview program was written to record and calculate the above information. To maximize the time efficiency of the program, it was separated into two different loops. One loop read all temperature and pressure probes and performed all necessary calculations. Again, to maximize the time efficiency, not every temperature and pressure probe was read each iteration. This loop ran at approximately 4 Hz. The other loop read the voltage from the strain gauges and converted it to the appropriate load (lift, drag or pitching moment). This loop ran at approximately 2/3 Hz. Figure 2-13 shows the front panel of the program designed for the wind tunnel tests at the University of Florida.

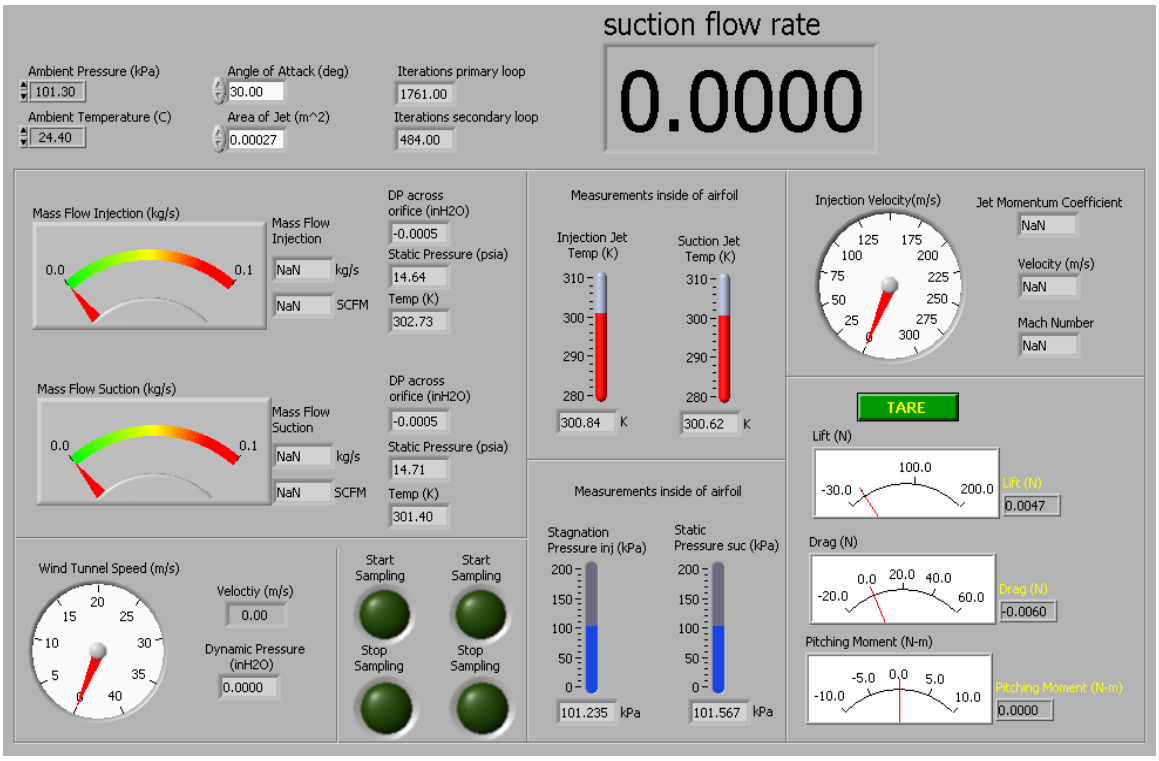

Figure 2-13. Program used in wind tunnel testing

The two Heise pressure transducers were sampled at approximately 2 Hz each. The pressures measured from the Heise include the injection static pressure, suction static pressure, the differential pressure across the orifice plates and the dynamic pressure of the wind tunnel. All values sampled from the Heise were averaged with the previous sample to filter out some of the noise.

The Druck pressure transducer was sampled at approximately 1 Hz. The pressure measurements from the Druck include the stagnation pressure in the injection slot and the static pressure in the suction manifold. All values sampled from the Druck were averaged with the previous sample to filter out some of the noise.

All temperature measurements were from a National Instruments SCXI -1000 unit. The program sampled this at approximately 1 Hz. The SCXI was connected to three T type and one K type thermocouples. The T type thermocouples were located in the injection duct of the airfoil, the suction duct of the airfoil and the suction pipe. The K type thermocouple was located in the injection pipe. The two thermocouples located in the pipes were used to gather the static temperature information for density calculations that went into mass flow rate calculations. Each temperature reading was given as a single value into the program from an average of 20 readings.

The second loop in the Labview program was used to sample the strain gauges used to calculate lift and drag. The strain measurements were given as a single value into the program. This number comes from the average of 5 integrations of a digital signal with a two-power line cycle integration time. The sampling rate is 300Hz. Two power line cycles is equal to 33.3ms; this comes to 10 samples for each integration. So, the voltage read into the program come from an average of 50 samples from the appropriate

Wheatstone bridge. The voltage is then turned into a force from the calibration curve previously found. This loop runs at approximately 2/3 Hz.

PIV images were also taken to better understand the flow field. The PIV images were taken separate from the other data recorded. The Labview program described above was used only to determine the wind tunnel velocity and mass flow rates for the PIV experiments. All other calculations were done on the computer designated for the PIV system.

Uncertainty Analysis

This section is dedicated to the uncertainty analysis of all measured and calculated values. The uncertainties of the measured values are determined first. The uncertainties of the calculated values are then found using the uncertainties of the measured values.

The measured uncertainties were found using equations 2-6, 2-7 and 2-8. In the equations U represents the total uncertainty, B represents the bias uncertainty and P represents the precision uncertainty. The uncertainties of the measured values are summarized in table 2-2.

$$U = \sqrt{B^2 + (t_{v,95}P)^2} \qquad \text{Eqn 2-6}$$

$$B = \sqrt{B_1^{\,2} + B_2^{\,2} + \ldots + B_M^{\,2}} \qquad \text{Eqn 2-7}$$

$$P = \sqrt{P_1^2 + P_2^{\,2} + \ldots + P_N^{\,2}} \qquad \text{Eqn 2-8}$$

The calculated uncertainties were found using equations 2-9 and 2-10.

$$R = R\left(x_1, x_2, \ldots, x_j\right) \qquad \text{Eqn 2-9}$$

$$U_R = \sqrt{\left(\frac{\partial R}{\partial x_1}U_{x_1}\right)^2 + \left(\frac{\partial R}{\partial x_2}U_{x_2}\right)^2 + \ldots + \left(\frac{\partial R}{\partial x_j}U_{x_j}\right)^2} \qquad \text{Eqn 2-10}$$

Table 2-2. List of the uncertainties of the measured values

Measurement	Uncertainty
Dynamic pressure from wind tunnel	0.014 inH_2O
Differential pressure across orifice plate	0.134 inH_2O
Static pressure in injection pipe	0.102 psi
Static pressure in suction pipe	0.092 psi
Stagnation pressure in injection slot	0.553 kPa
Static pressure in suction manifold	0.295 kPa
Static temperature in injection pipe	1.170 C
Static temperature in suction pipe	0.730 C
Static temperature in injection duct of airfoil	0.730 C
Static temperature in suction duct of airfoil	0.730 C
Lift force, C_l	0.0088-0.043
Drag force, C_d	0.0088-0.043

The wind tunnel velocity is found from the dynamic pressure. The velocity was calculated using equation 2-11.

$$v = \sqrt{\frac{2q}{\rho}} \qquad \text{Eqn 2-11}$$

where,

v Wind tunnel velocity
q Dynamic pressure
ρ Density of free stream

The uncertainty in the velocity measurement reduces to equations 2-12. The uncertainty in the velocity measurement is 0.748 m/s or 2.08%. The velocity of the wind tunnel was also checked with PIV. The velocity measured from PIV was within the uncertainty.

$$U_v = \sqrt{\left(\frac{\partial v}{\partial q}U_q\right)^2 + \left(\frac{\partial v}{\partial \rho}U_\rho\right)^2} \qquad \text{Eqn 2-12}$$

The mass flow rate was given by equation 2-1. The uncertainty of the mass flow rate can be reduced to equation 2-13. Table 2-3 shows values for the given uncertainties.

$$\frac{\partial q_m}{q_m} = \left(\left(\frac{\partial C}{C}\right)^2 + \left(\frac{\partial \varepsilon}{\varepsilon}\right)^2 + \left(\frac{2\beta^4}{1-\beta^4}\right)^2 \left(\frac{\partial D}{D}\right)^2 + \left(\frac{2}{1-\beta^4}\right)^2 \left(\frac{\partial d}{d}\right)^2 + \frac{1}{4}\left(\frac{\partial \Delta p}{\Delta p}\right)^2 + \frac{1}{4}\left(\frac{\partial \rho_1}{\rho_1}\right)^2 \right)^{\frac{1}{2}} \quad \text{Eqn 2-13}$$

Table 2-3. Uncertainty in orifice plate calculation

Coefficient	Uncertainty of Injection Side, %	Uncertainty of Suction Side, %
$\frac{\partial C}{C}$	0.06	0.06
$\frac{\partial \varepsilon}{\varepsilon}$	0.144	0.144
$\left(\frac{2\beta^4}{1-\beta^4}\right)^2 \left(\frac{\partial D}{D}\right)^2$	≈ 0	≈ 0
$\left(\frac{2}{1-\beta^4}\right)^2 \left(\frac{\partial d}{d}\right)^2$	≈ 0	≈ 0
$\frac{\partial \Delta p}{\Delta p}$	1.914	2.197
$\frac{\partial \rho_1}{\rho_1} = \sqrt{\left(\frac{\partial p_1}{p_1}\right)^2 + \left(\frac{\partial T_1}{T_1}\right)^2}$	0.562	0.870

The uncertainty in the mass flow rate measurement is 1.01% for the injection and 1.19% for the suction.

The uncertainty in A/A* needs to be found before the uncertainty of the injection velocity can be determined. Equation 2-3 defined A/A*. The uncertainty of this ratio is given in equation 2-14.

$$U_{A/A^*} = \sqrt{\left(\frac{\partial (A/A^*)}{\partial P_0} U_{P_0}\right)^2 + \left(\frac{\partial (A/A^*)}{\partial q_m} U_{q_m}\right)^2 + \left(\frac{\partial (A/A^*)}{\partial T_0} U_{T_0}\right)^2} \quad \text{Eqn 2-14}$$

The uncertainty in A/A* is calculated to be 1.37 %. This relates to an uncertainty in the Mach number of 1.65%. This uncertainty relates directly to the uncertainty of the velocity because the speed of sound, a, is considered constant. So the uncertainty of the injection velocity is 1.65%.

The jet momentum coefficient is the last quantity for which the uncertainty needs to be calculated. The jet momentum coefficient was defined in equation 2-5. The uncertainty of the jet momentum coefficient is given by equation 2-15.

$$U_{C_\mu} = \sqrt{\left(\frac{\partial(C_\mu)}{\partial v_{jet}} U_{v_{jet}}\right)^2 + \left(\frac{\partial(C_\mu)}{\partial q_m} U_{q_m}\right)^2 + \left(\frac{\partial(C_\mu)}{\partial v_\infty} U_{v_\infty}\right)^2} \qquad \text{Eqn 2-15}$$

The uncertainty of the jet momentum coefficient is calculated to be 4.59%.

The uncertainty of the lift and drag was calculated using Student's t-distribution [15], which is given in equation 2-16. Student's t-distribution gives the uncertainty of the true mean.

$$\Delta = \frac{t\sigma}{\sqrt{n}} \qquad \text{Eqn 2-16}$$

where,

Δ	Uncertainty
t	t-value for corresponding confidence level
σ	Standard deviation
n	Number of samples

For a 95% confidence level and 50 samples, the t-value is equal to 2.0105. The standard deviation for both lift and drag at lower angle of attacks is 1 N and at higher angle of attacks is 5 N. This corresponds to standard deviation in terms of C_l and C_d of 0.031-0.153. So, the uncertainty in C_l and C_d would then be 0.0088 at lower angle of attacks and 0.043 at higher angle of attacks.

The uncertainty of the PIV measurements was calculated as well. The pixel resolution of the camera and the resolution of the calibration ruler were the dominant terms of the uncertainty; they were .1mm and .25mm respectively. This results in an uncertainty of 1.00 m/s or 2.79%.

CHAPTER 3
PROCEDURE

This chapter describes the experimental procedure followed during the testing of the CFJ airfoils. The airfoils were tested in three configurations. The CFJ0025-065-196 and CFJ0025-131-196 were tested along with a baseline airfoil. The baseline airfoil was really the CFJ0025-131-196 airfoil with an insert that slides into the injection and suction slots and fills the recessed portion. The profile of the airfoil with the filler piece installed was a NACA 0025.

The airfoils were also tested in two different manners. The airfoils were tested for lift and drag characteristics with strain gauges and flow field visualization with particle image velocimetry.

The lift and drag testing is discussed first. A rigorous airfoil assembly procedure and testing procedure can be found in appendix C and appendix D respectively.

The airfoil to be tested would have to be assembled and placed into the wind tunnel. Although there were two different airfoils, they shared the same endplates and aluminum foam insert. Therefore changing airfoils was somewhat laborious. The airfoil would have to be disassembled and the new airfoil reassembled. Once the airfoil was in the wind tunnel, the procedure was as follows:

1. Turn on vacuum pump and begin pulling vacuum
2. Start compressor
3. Connect different probes to appropriate transducers
4. Turn on all instrumentation and computer
5. Start Labview program written for testing
6. Make sure all probes are reading correctly in Labview VI
7. Set zero degree angle of attack

8. Rotate airfoil to desired angle of attack
9. Enter necessary information into the program
10. Turn on wind tunnel
11. Start air injection
12. Dial in suction mass flow rate
13. Only continue after the suction mass flow rate is desirable
14. Start air suction and sampling

The Labview program recorded the following measured values:

1. Static pressure upstream of injection orifice plate
2. Static temperature upstream of injection orifice plate
3. Differential pressure across injection orifice plate
4. Static pressure upstream of suction orifice plate
5. Static temperature upstream of suction orifice plate
6. Differential pressure across suction orifice plate
7. Static temperature in airfoil injection duct
8. Static temperature in airfoil suction duct
9. Stagnation pressure at injection slot
10. Static pressure in suction manifold
11. Lift force
12. Drag force

The Labview program recorded the following calculated values:

1. Mass flow rate of air pushed through injection slot
2. Mass flow rate of air pulled through suction slot
3. Wind tunnel velocity
4. Injection jet velocity
5. Injection jet momentum coefficient

Other useful information the Labview program recorded:

1. The time of the primary loop
2. The time of the secondary loop
3. Angle of attack

The times of the primary loop and secondary loop were important because the two loops run at different speeds. The time was then a way to relate the information in both loops together. The angle of attack was also convenient to have in the file. The only other place the angle of attack was saved was in the file name itself.

The PIV testing was similar to the lift and drag testing. The testing procedure was as follows:

1. Steps 1-13 are identical
2. Adjust laser light sheet to illuminate desired plane
3. Set the laser and camera timing for wind tunnel velocity and spatial resolution
4. Calibrate PIV with ruler by placing it in the light sheet and focus camera on ruler
5. Turn on fog machine
6. Adjust seeding particles until images are clear and filled with fog
7. Turn on suction and capture PIV images

CHAPTER 4
DISCUSSION OF RESULTS

This chapter is dedicated to the results from the wind tunnel tests conducted at the University of Florida. This chapter includes tests taken for lift and drag measurements as well as tests taken for flow field visualization. The CFJ airfoil was tested in many ways. These will all be described in detail in this chapter.

Different Tests Conducted

The three different airfoils were tested in many different manners. The airfoils were tested to study things such as lift, drag, stall angle, velocity profile, stagnation point location, effects of leading edge trip, separation due to high injection mass flow rate and effects of lift and drag due to altered mass flow rates. Two test matrices are shown in tables 4-1 and 4-2. The matrices are a complete record of all wind tunnel tests conducted at the University of Florida.

Many of the different testing manners are discussed in the following sections. The two tests that are not discussed later are the leading edge trip and the tests run without the wind tunnel on. The reasons for these tests will be explained in this section.

The airfoils were tested with and without a leading edge trip. The trip was applied by spraying the leading edge of the airfoil with a strip of photo adhesive. The width of the strip was 1/2" or 8.33% chord length. Immediately after the adhesive was applied, fine sand was sprinkled over it. The trip was then left to dry.

The purpose of the leading edge trip was to transition the flow from laminar to turbulent. The 0.1527m chord length gives the airfoil a Reynolds number around

Table 4-1. Lift and drag test matrix

	-10	-5	0	5	10	11	12	13	14	15	16	17	18	19	20	22	24	25	26	28	30	31	32	33	34	35	36	37	38	39	40	41	42	43	44	45
1mm Data																																				
no suction & no tunnel			D		D										D						D						D			D						
.045 kg/s			D		D										D						D						D			D						
.045 kg/s no suction			D		D										D						D						D			D						
.045 kg/s no tunnel			D		D										D						D						D			D						
no injection or suction	D	D	D	D	D	D	D	D	D	D	D	D	D	D	D	D	D		D	D	D															
.030 kg/s w/trip	D		D		D										D						D					D		D	D	D						
.045 kg/s w/trip	D		D		D										D						D					D				D		D	D			
.052 kg/s w/trip	D		D		D										D						D					D		D		D				D	D	D
.17 jmc #1	D	D	D	D	D					D					D		D		D	D	D															
.17 jmc #2	D	D	D	D	D					D					D		D		D	D																
119 kPa stag pressure #1	D	D	D	D	D					D					D		D		D	D	D					D		D	D							
119 kPa stag pressure #2	D	D	D	D	D					D					D		D		D	D	D															
2mm Data																																				
no suction & no tunnel			D												D						D															
.08 kg/s			D												D						D															
.08 kg/s no suction			D												D						D															
.08 kg/s no tunnel			D												D						D															
no injection or suction	D	D	D	D	D		D	D	D	D					D			D			D															
no injection or suction w/trip	D		D					D	D	D	D	D	D		D						D	D	D	D	D	D	D		D	D						
.06 kg/s w/trip	D		D		D										D						D	D	D	D												
.08 kg/s w/trip	D		D		D										D						D				D	D	D									
.11 kg/s w/trip	D		D		D										D						D					D			D	D						
.11 kg/s	D		D		D										D						D															
Baseline Data																																				
baseline #1	D	D	D	D	D					D					D		D		D	D	D															
baseline #2	D	D	D	D	D					D					D		D		D	D	D															
baseline #3			D		D				D		D	D	D	D	D	D	D		D	D	D															
baseline #4			D	D	D					D	D	D	D	D	D			D			D															
baseline #5			D	D	D							D			D																					
baseline w/trip	D	D	D	D	D					D		D	D	D	D			D			D															

Table 4-2. PIV test matrix

Description \ AOA	0	10	20	30	36	40	43
Baseline, whole airfoil		D	D				
Baseline, TE	D	D	D				
Baseline, wake	D	D	D				
1mm, whole airfoil	D	D		D		D	D
1mm, TE	D	D		D		D	D
1mm, wake	D	D		D		D	D
1mm, zoomed inj	did not work, no seed particles in flow						
1mm, zoomed suc	D		D			D	
1mm, zoomed stag pt	D	D	D/various	D/various			
1mm, seperation				D			
2mm, whole airfoil	D	D		D	D		D
2mm, TE	D	D		D	D		D
2mm, wake	D	D		D	D		D
2mm, zoomed inj	D		D				
2mm, zoomed suc	D		D				
D = Done							
N = Need							
D / various = Did various mdot							

380,000. The injection jet's turbulence would easily turn this laminar flow to a turbulent flow where as the flow over the NACA 0025 would remain in the laminar region the majority of the distance over the airfoil. Comparing a dominantly laminar flow to a turbulent flow would then lead to erroneous conclusions.

The airfoil was also tested with and without the wind tunnel turned on. The reason for this was to see the contribution of the jets momentum on the lift measurement. The ratio of lift with the jets on and tunnel off to lift with jets on and tunnel on was summarized in table 4-3. It was concluded the overall aerodynamics of the airfoil are to be credited with the lift measurement and not the momentum flux of the injection and suction jets.

Table 4-3. Ratio of lift with tunnel off to lift with tunnel on

Description/AOA	0 deg	20 deg	30 deg	36 deg
CFJ0025-065-196	0.269	0.076	0.069	0.063
CFJ0025-131-196	0.358	0.088	0.099	N/A

Improved Lift, Drag and Stall

During the lift and drag measurements, the stagnation pressure of the injection jet dictated the mass flow rate. For both airfoils, CFJ0025-065-196 and CFJ0025-131-196, the desired mass flow rate was dialed in when the airfoil was at 30 degrees angle of attack. This stagnation pressure was the pressure at which all other angles of attack were run. So, the mass flow rate did vary slightly depending on the angle of attack.

Figure 4-1 is a summary of the CFJ0025-065-196 lift performance. It can be seen that the higher mass flow rates have a higher lift coefficient and stall margin. This is not a surprising result. When the mass flow was raised, the jet momentum coefficient was raised; meaning the amount of momentum injected into the flow was higher. Also plotted is the performance of the NACA 0025 for comparison.

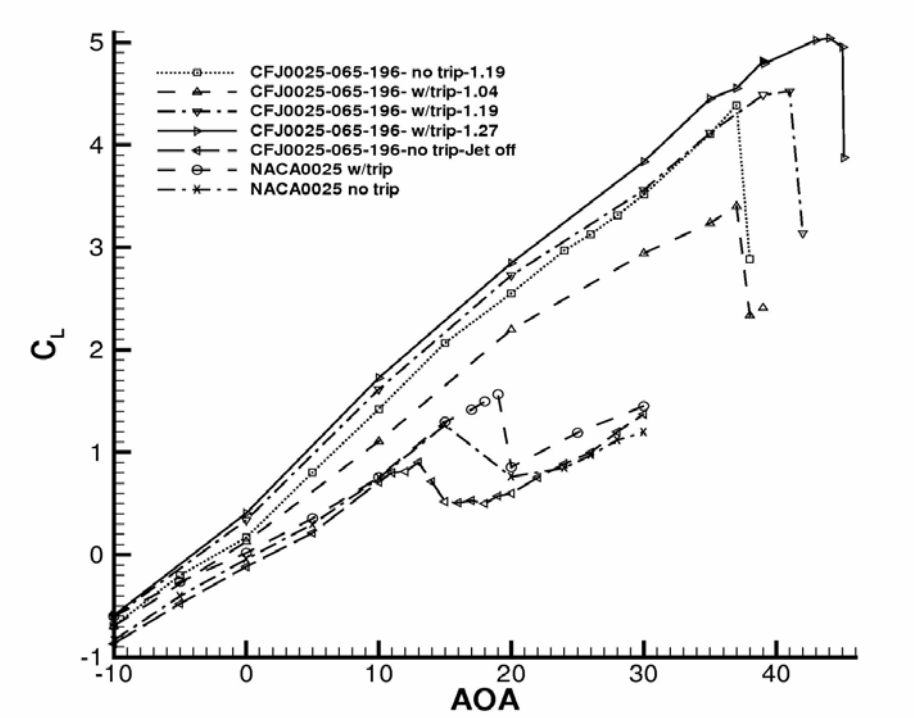

Figure 4-1. Lift coefficient verse angle of attack for CFJ0025-065-196

The effect of the boundary layer trip can also be seen in figure 4-1. The stall margin of the NACA 0025 and the CFJ0025-065-196 (stagnation pressure ratio of 1.19) was increased by 4 degrees each when the leading edge trip was applied. The bottom curve in the figure is the CFJ0025-065-196 with no boundary layer trip and the jets turned off. It is easy to see the effect the jets have on the aerodynamics of the airfoil.

Table 4-4 is a comparison between all three airfoil configurations. The values for the CFJ0025-065-196 are from the maximum flow rate tested, which corresponds to a stagnation pressure ratio of 1.27. It can be seen the maximum lift coefficient for the CFJ0025-065-196 airfoil is 3.2 times as large as the maximum lift coefficient for the NACA 0025. This is an improvement of 220%. Other important parameters are the angle of attack at which separation occurs is increased by 132% and the minimum drag coefficient goes from positive to negative.

Table 4-4. Comparison between CFJ airfoils and baseline airfoil

Airfoil	$AOA_{C_L=0}$ (deg)	$AOA_{C_{L\max}}$ (deg)	$C_{L\max}$	$C_{D\min}$
NACA 0025	0	19	1.57	0.128
CFJ0025-065-196	-4	44	5.04	-0.036
CFJ0025-131-196	-6.5	38	4.90	-0.263

The drag polar is also plotted for the CFJ0025-065-196 airfoil in figure 4-2. The most notable aspect of the drag polar is the negative drag for the CFJ airfoil at low angles of attack. Negative drag is equivalent to thrust. The injection jet momentum coefficient that enabled these dramatic increases in lift and stall margin and decrease in drag are given in figure 4-3.

The same plots were constructed with the CFJ0025-131-196 airfoil. Again, the CFJ0025-131-196 is a similar airfoil with twice as large of an injection slot. The suction slots are the same size. Because the injection jet is twice as large, the mass flow rates are about twice as large.

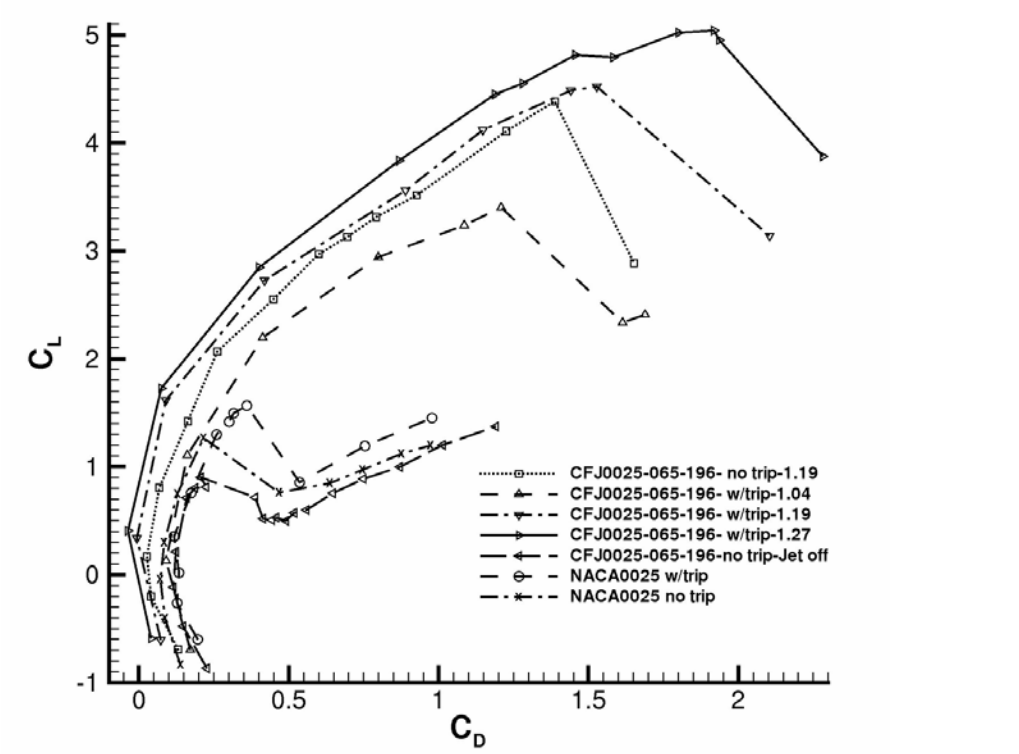

Figure 4-2. Drag polar for CFJ0025-065-196

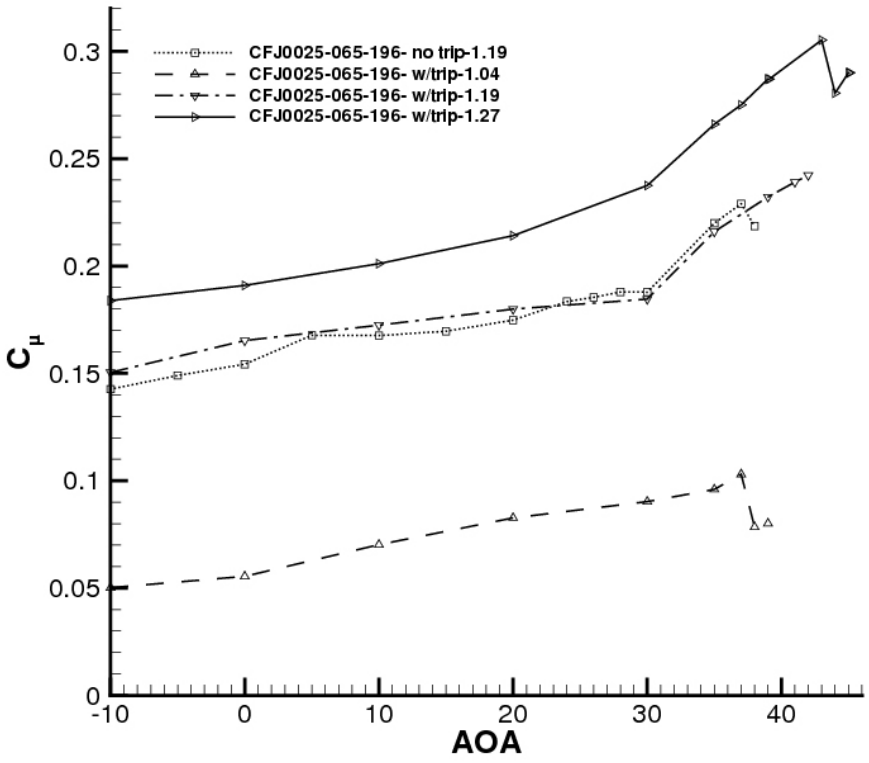

Figure 4-3. Injection jet coefficients of CFJ0025-065-196

The performance of the CFJ0025-131-196 airfoil was very similar to the CFJ0025-065-196 airfoil. The main differences being a slightly lower $C_{L\max}$, $AOA_{C_{L\max}}$ and $C_{D\min}$. The CFJ0025-131-196 was also compared to the other two airfoils configurations in table 4-4. Figure 4-4 is a summary of the CFJ0025-131-196 lift performance. The drag polar is also plotted for the CFJ0025-131-196 airfoil in figure 4-5. The injection jet momentum coefficient that enabled these dramatic increases in lift and stall margin and decrease in drag are given in figure 4-6.

It can be seen the CFJ airfoils dramatically increase lift, increase stall margin and decrease drag. The CFJ0025-065-196 airfoil appears superior for increased lift and stall margin, while the CFJ0025-131-196 appears superior for decreased drag. There is still much future optimization that needs to be done.

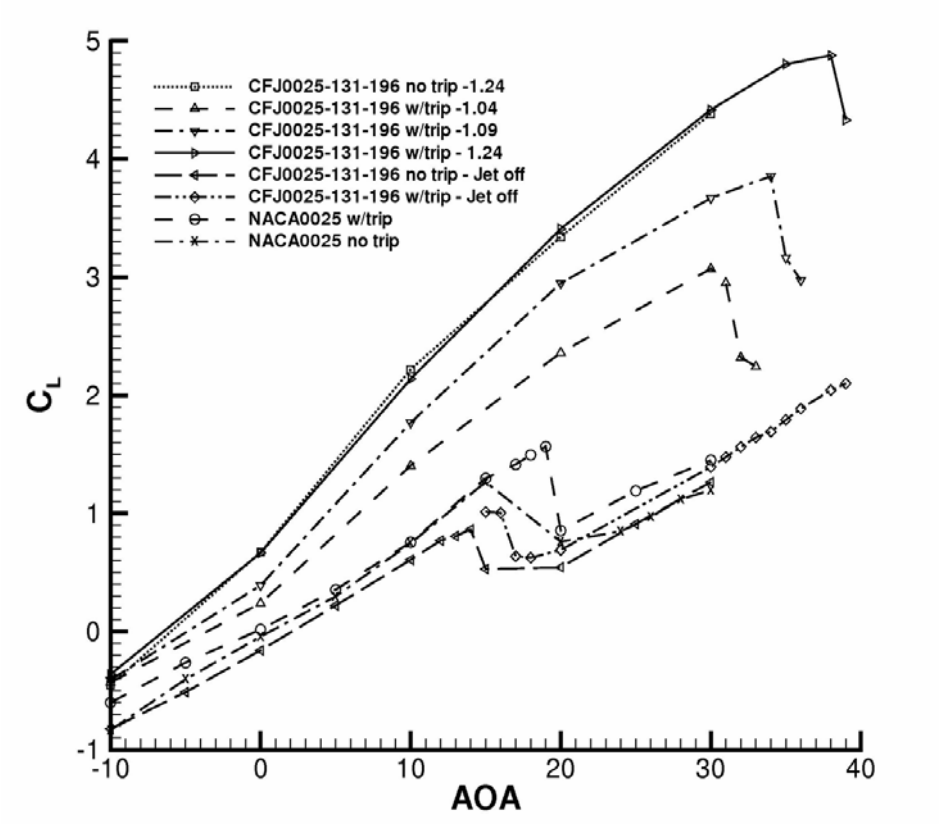

Figure 4-4. Lift coefficient verse angle of attack for CFJ0025-131-196

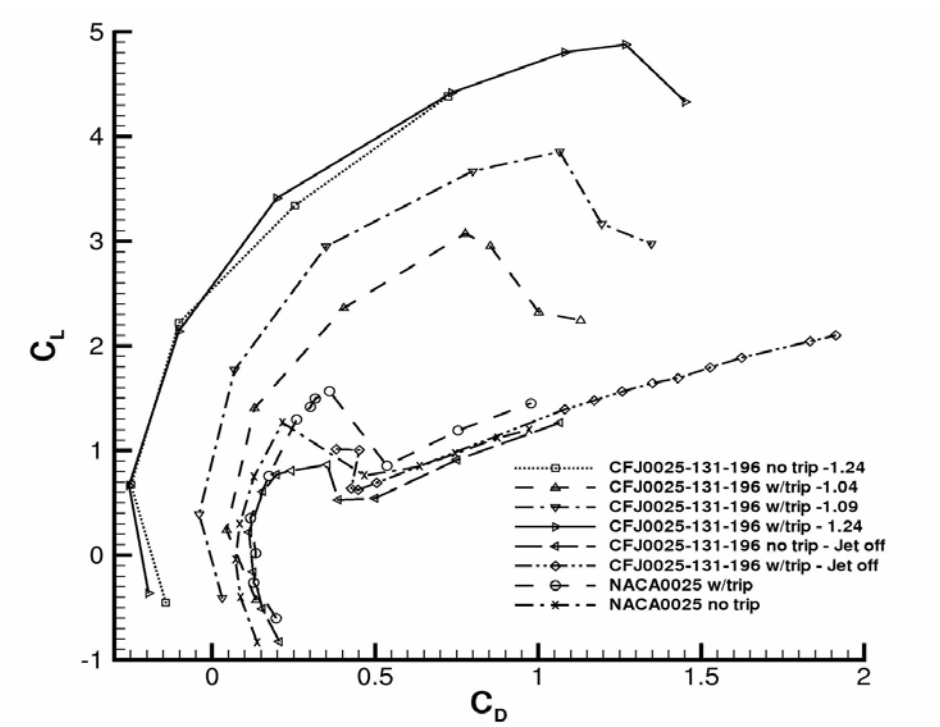

Figure 4-5. Drag polar for CFJ0025-131-196

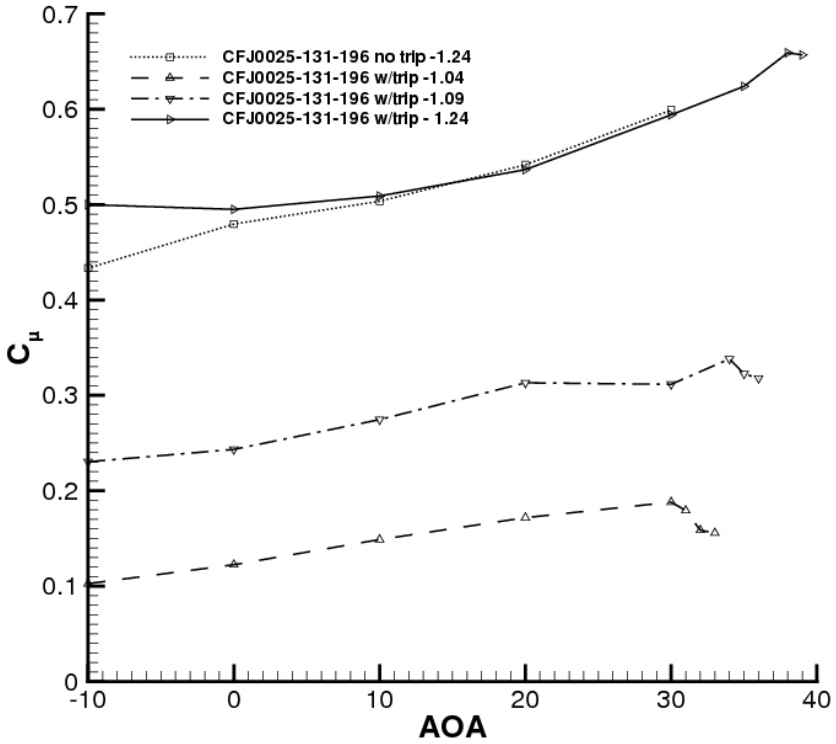

Figure 4-6. Injection jet coefficients of CFJ0025-131-196

Instability of the Jet

As the mass flow rate of the jets was increased, the performance of the CFJ airfoil increased. But for the CFJ0025-065-196 airfoil, there was a maximum to this mass flow rate. The injection jet lost the ability to stay attached to the airfoil when it was forced passed this maximum. The flow would become separated from the airfoil and recirculation would occur. The result was loss of lift and increased drag.

The mass flow rate of the suction jet was not capable of being adjusted accurately while tests were being conducted. For this reason, only the injection jet was used in the tests that looked at the stability of the flow.

It is still unknown what exactly is causing this instability. It is thought that the tangential momentum of the injection jet becomes too large and the flow can no longer follow the curvature to the airfoil.

It is unknown if the same would be true for the CFJ0025-131-196 airfoil. Limitations on the orifice plate and differential pressure transducer, which were both used to measure the mass flow rate, made it impossible to force separation. The mass flow rate just could not be pushed high enough and measured with the current setup.

Stagnation Point Location

The stagnation point was also looked at for different mass flow rates. The stagnation point lies on the pressure surface of the CFJ airfoil. Due to limitations with the PIV set up, only the flow field over the suction surface could be viewed. Therefore, the exact location of the stagnation point could not be captured; however, evidence of the movement from altering the mass flow rates was.

Figure 4-7 and 4-8 show the flow field of the CFJ0025-065-196 at 20 and 30 degrees angle of attack, respectively. It can be seen that the stagnation point shifts along the pressure surface of the airfoil as the mass flow rate is increased. This is apparent in both cases. The result of the stagnation point shifting, as the mass flow rate increases, is higher velocities at the leading edge and over the suction surface, which leads to higher lift. Future design will include a way to capture PIV images on the pressure surface of the airfoil.

PIV Results

Too much PIV data was taken to include it all in this thesis. Because of this only a few interesting cases will be shown (appendix E includes additional images). The PIV images in this thesis have had the appropriate airfoil superimposed onto them. The placement of the airfoil is not exact but a best estimate of the proper location. The images are also averaged from 75-120 images. A fog machine was used to generate seeding particle on the order of 1-10 microns. The camera used to capture the images

had a resolution of 1600x1200 pixels. This results in a resolution of approximately 1.7mm for the PIV images of the whole airfoil using an interrogation region of 16x16 pixels.

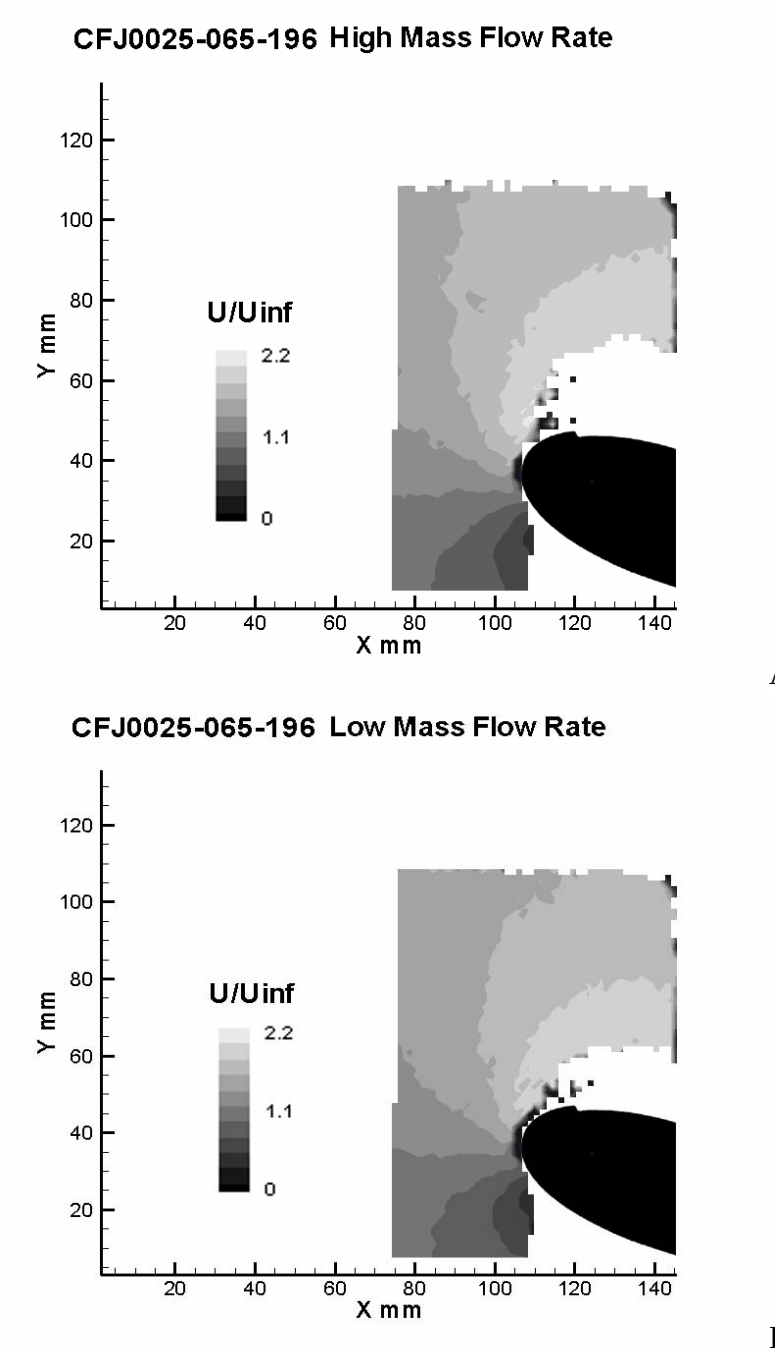

Figure 4-7. Stagnation point location for CFJ0025-065-196 at 20 degrees angle of attack and A) high and B) low mass flow rates

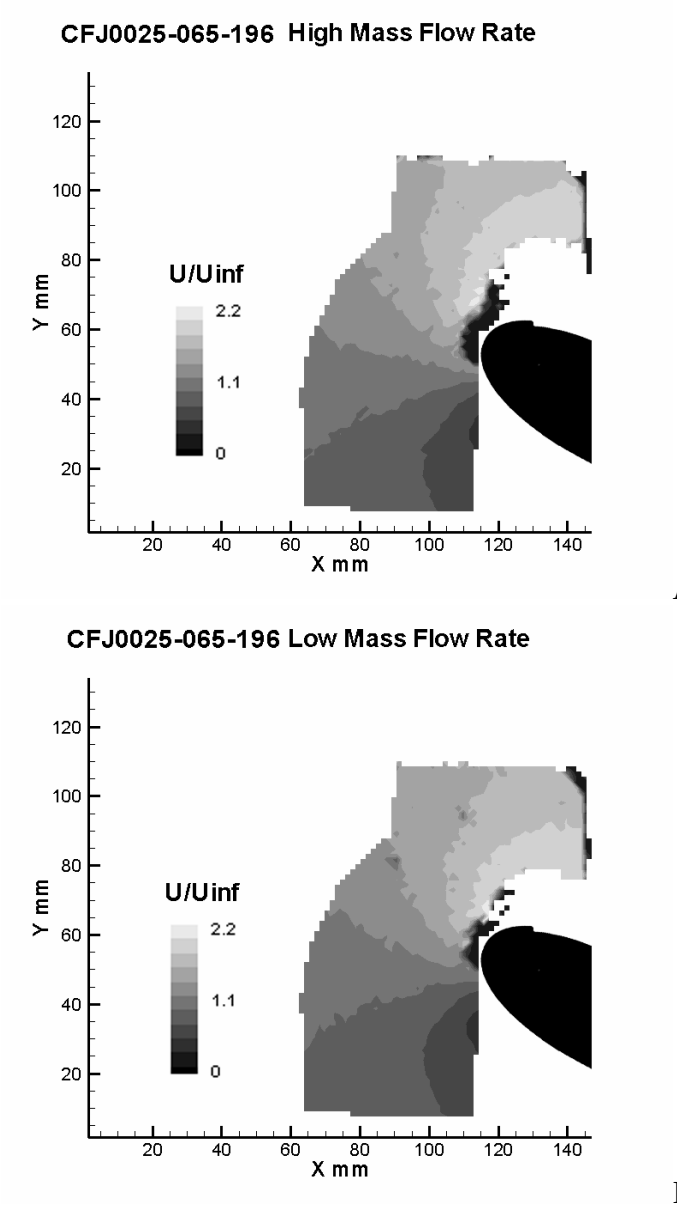

Figure 4-8. Stagnation point location for CFJ0025-065-196 at 30 degrees angle of attack and A) high and B) low mass flow rates

It can be seen from the streamlines in figure 4-9 that the flow is attached at 40 degrees angle of attack and separated at 43 degrees for the CFJ0025-065-196 airfoil. The airfoils did not utilize a boundary layer trip. The trip adds about 4 degrees to the stall angle; therefore the data is in agreement with the data form the lift and drag tests for the stall angle. Figure 4-10 shows the flow over the CFJ0025-131-196 airfoil is attached at

36 degrees angle of attack and detached at 43 degrees. Figure 4-11 show the same for the NACA 0025, attached at 10 degrees angle of attack and detached at 20 degrees.

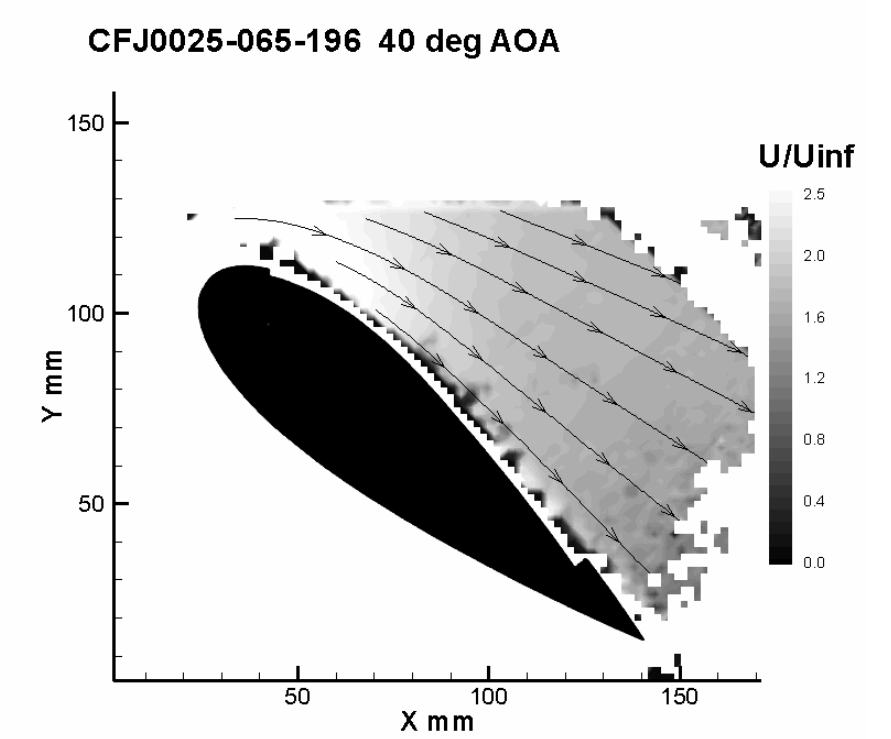

A

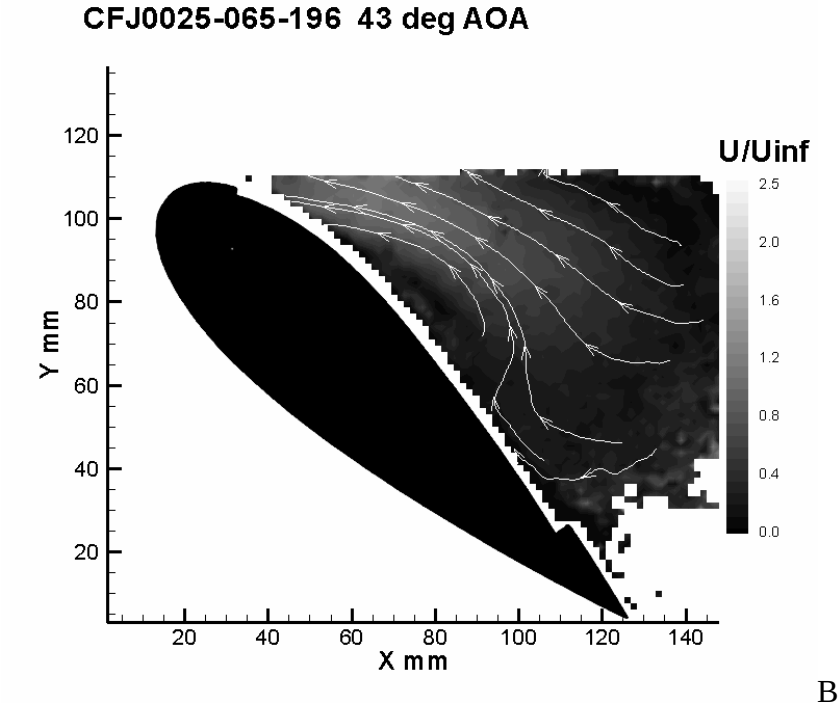

B

Figure 4-9. PIV image of flow over CFJ0025-065-196 A) 40 deg and B) 43 deg

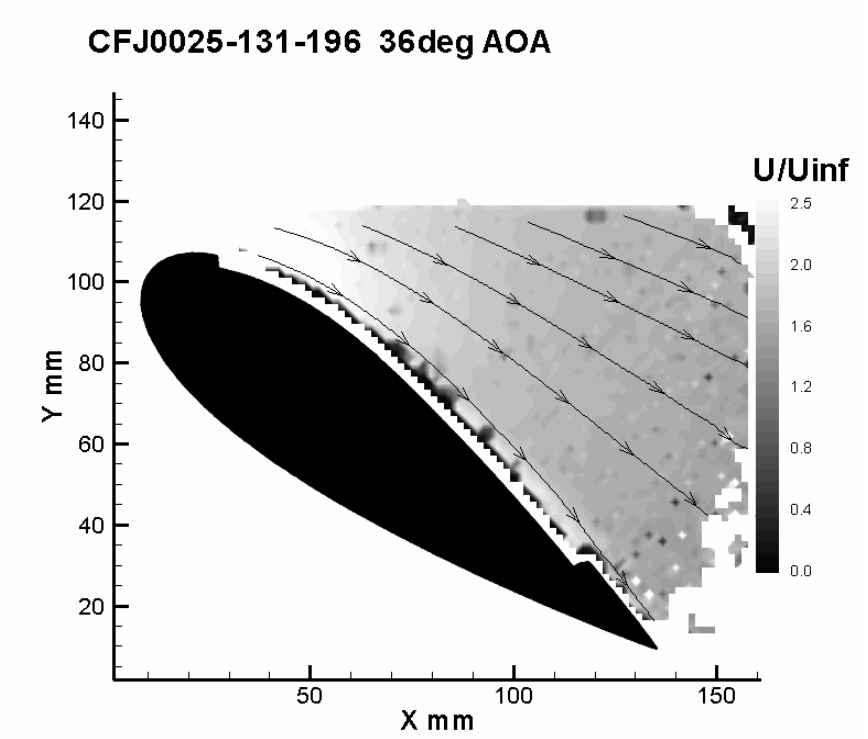

A

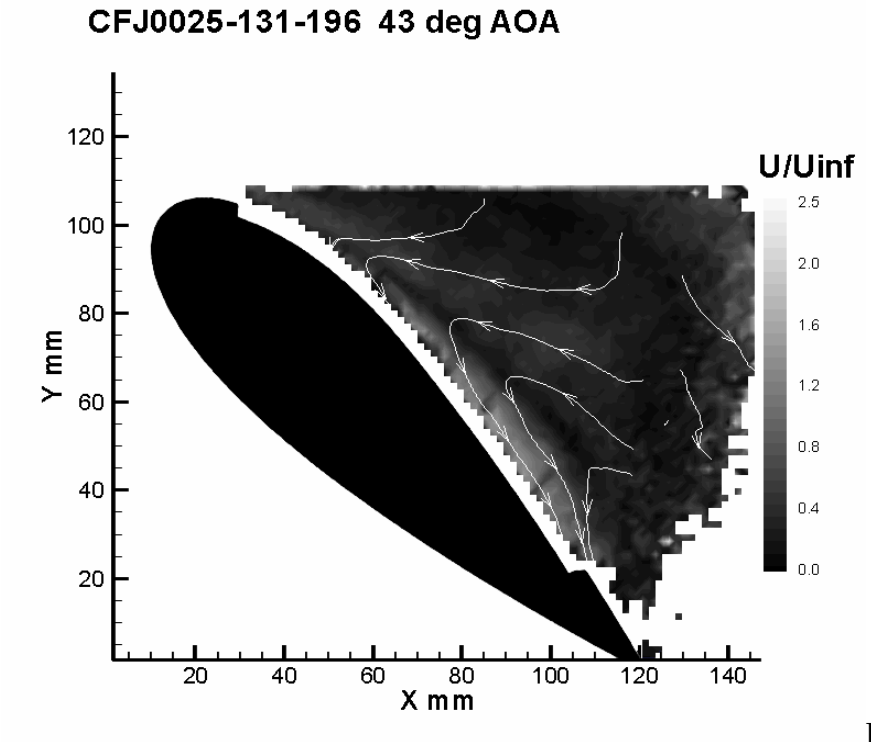

B

Figure 4-10. PIV image of flow over CFJ0025-131-196 A) 36 deg and B) 43 deg

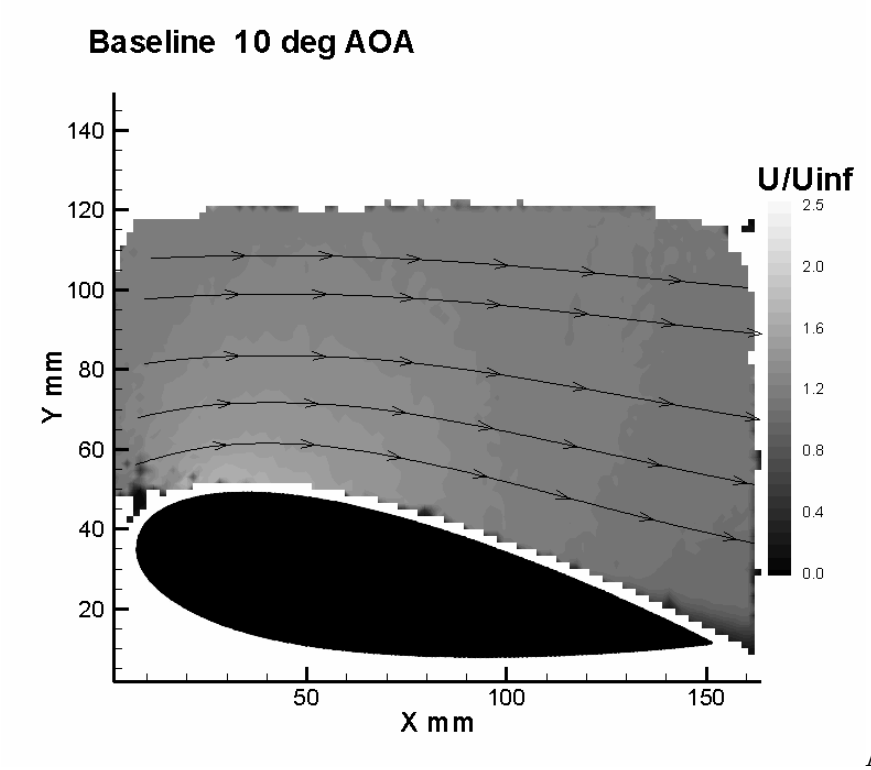

A

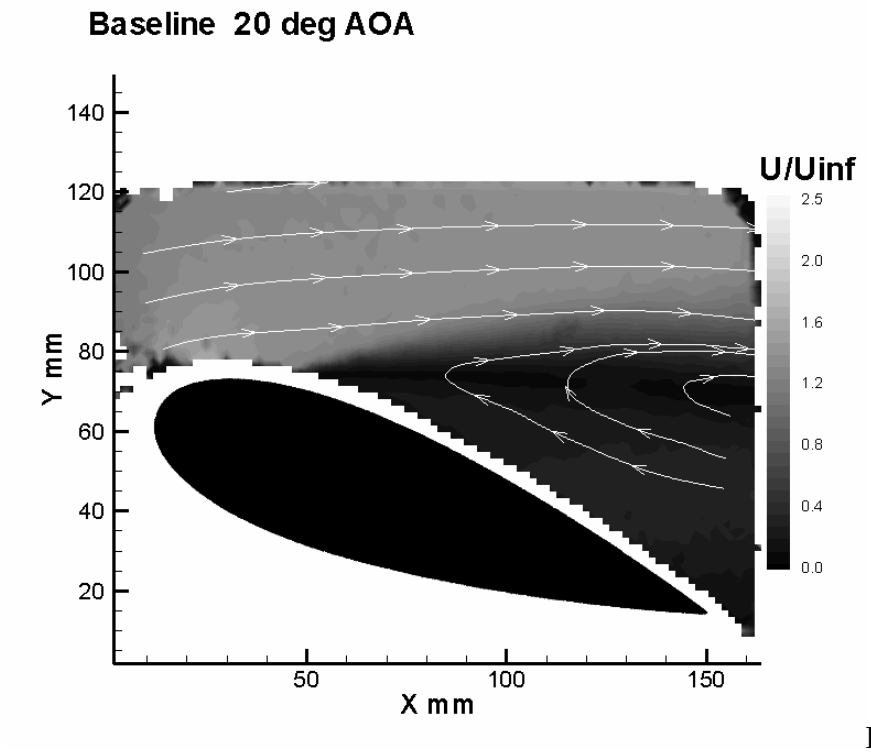

B

Figure 4-11. PIV image of flow over baseline airfoil A) 10 deg and B) 20 deg

Velocity profiles were constructed from the PIV data as well. Figure 4-12 is a group of velocity profiles comparing the flow over the baseline, the CFJ0025-065-196 and the CFJ0025-131-196 airfoils at 10 degrees angle of attack and various chord locations (5%, 15%, 30%, 50%, 75%, 100%). The profiles were taken perpendicular to the airfoil's surface. The x-axis in the profiles is a dimensionless velocity. It is the local velocity over the airfoil normalized by the free stream velocity. The y-axis is the distance from the surface of the airfoil given in percent chord length. In the legend, base refers to the baseline airfoil, 0.65% refers to the CFJ0025-065-196 airfoil and 1.31% refers to the CFJ0025-131-196 airfoil.

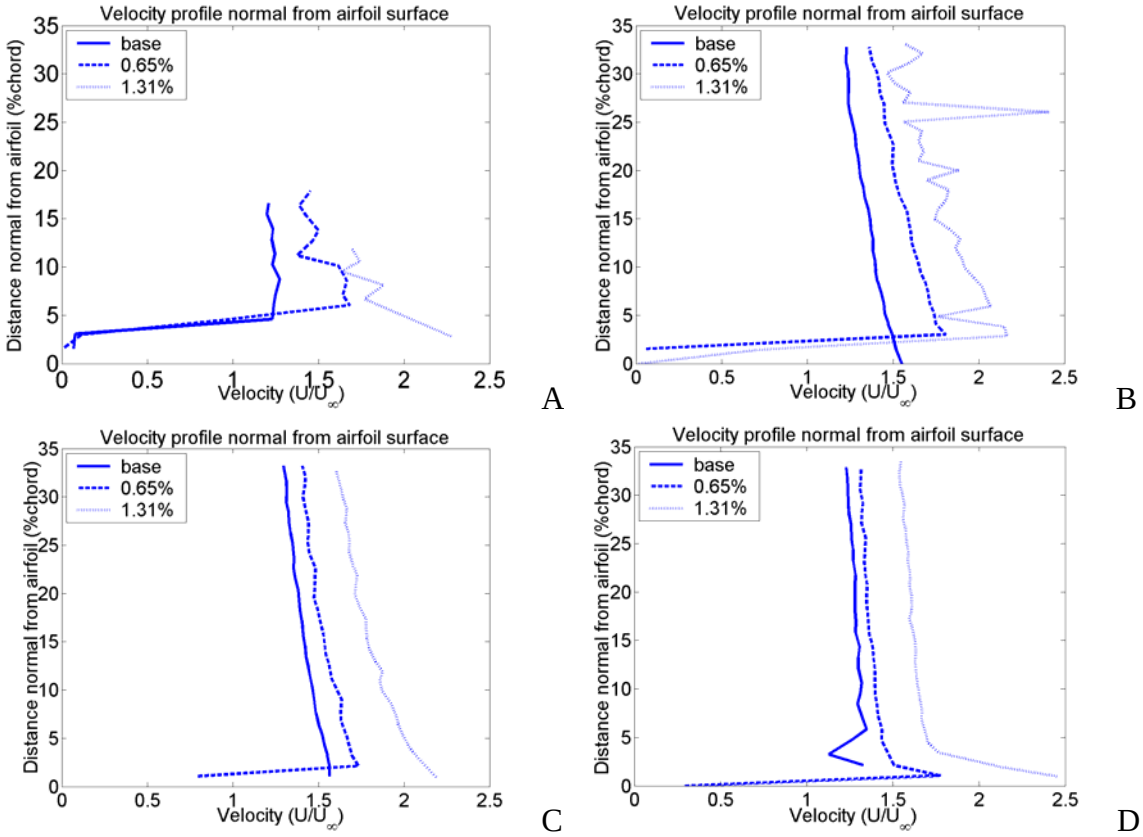

Figure 4-12. Velocity profiles of baseline airfoil, CFJ0025-065-196 and CFJ0025-131-196 at 10 degree AOA and various chord locations, A) 5% B) 15% C) 30% D) 50% E) 75% F) 100%

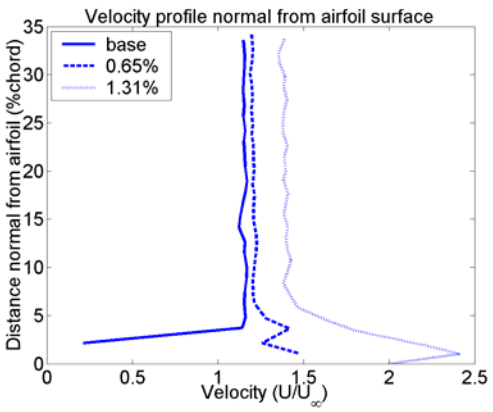

E

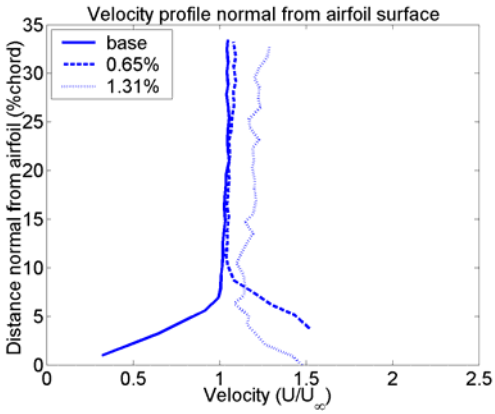

F

Figure 4-12. Continued

Figure 4-13 groups all velocity profiles into a single graph so the flow trend is more visible and figure 4-14 illustrates the position where the profiles were taken from.

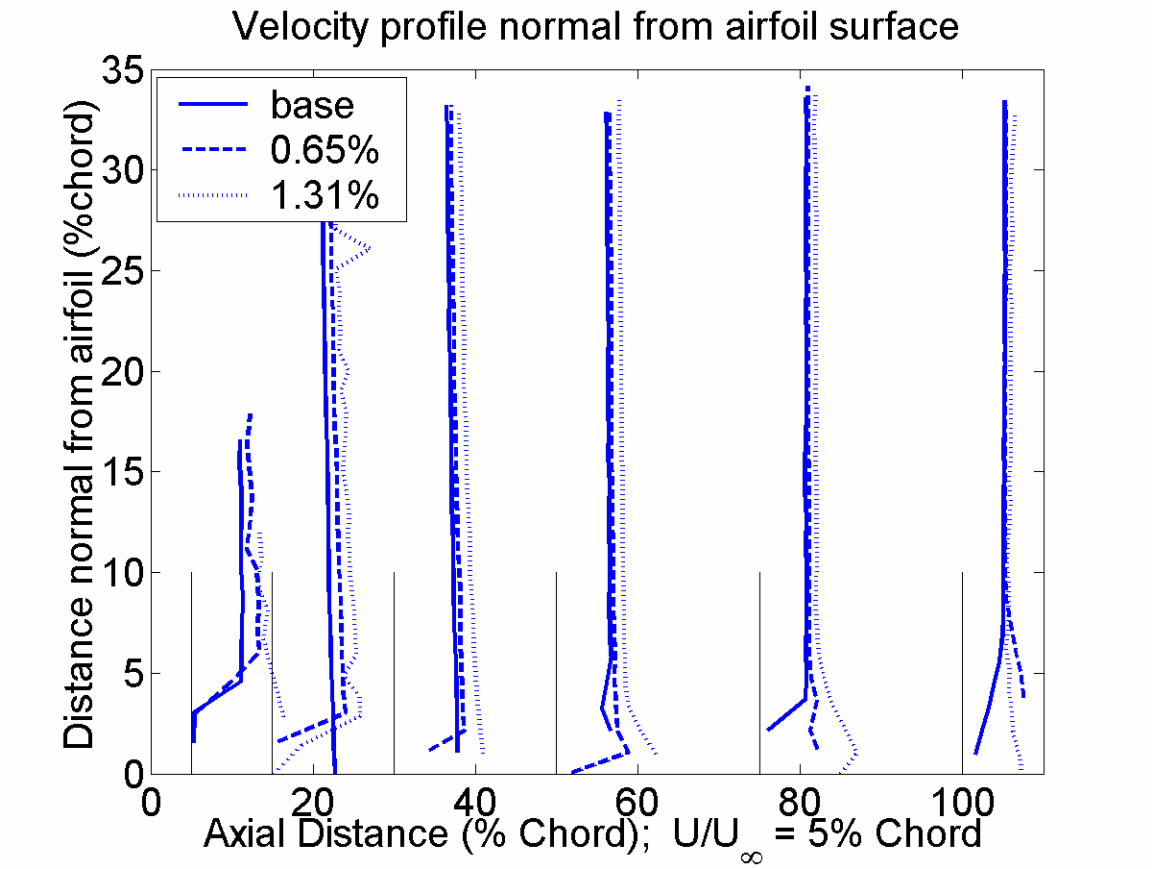

Figure 4-13. Velocity profiles of baseline airfoil, CFJ0025-065-196 and CFJ0025-131-196 combined into single graph (10 degree AOA)

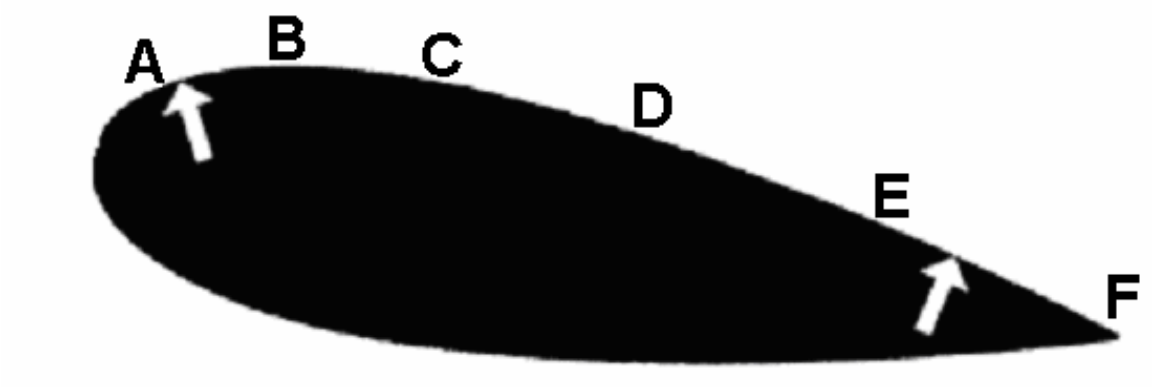

Figure 4-14. Positions from where velocity profiles where taken. The arrows designate the location of the injection and suction slots.

The effects of the injection and suction jets can be seen in the velocity profiles. The CFJ0025-065-196 airfoil has a larger velocity over the fore half of the airfoil compared to the baseline. The CFJ0025-131-196 has a significantly larger velocity over the entire airfoil compared to the baseline and CFJ0025-065-196 airfoils.

It should be noted that the reason that some of the velocity profiles are discontinuous around 0-5% chord lengths is not necessarily due to any boundary condition or the jets, but instead it is a result of the PIV camera and seeding particle. There was a considerable amount of reflection that comes off the aluminum airfoil that caused excess noise. Also no seeding particles were used in the injection system.

Figure 4-15 is a group of velocity profiles comparing the flow over the CFJ0025-065-196 airfoil and the CFJ0025-131-196 airfoil at the same locations as before and 30 degrees angle of attack. The profile at the trailing edge is not included because the image had a lot of reflection from the Plexiglas and back walls. Therefore the data is considered invalid. Figure 4-16 is all of the profiles grouped together so the flow trend is more visible. Again it can be seen that the result of the larger injection slot is a greater velocity over the entire airfoil.

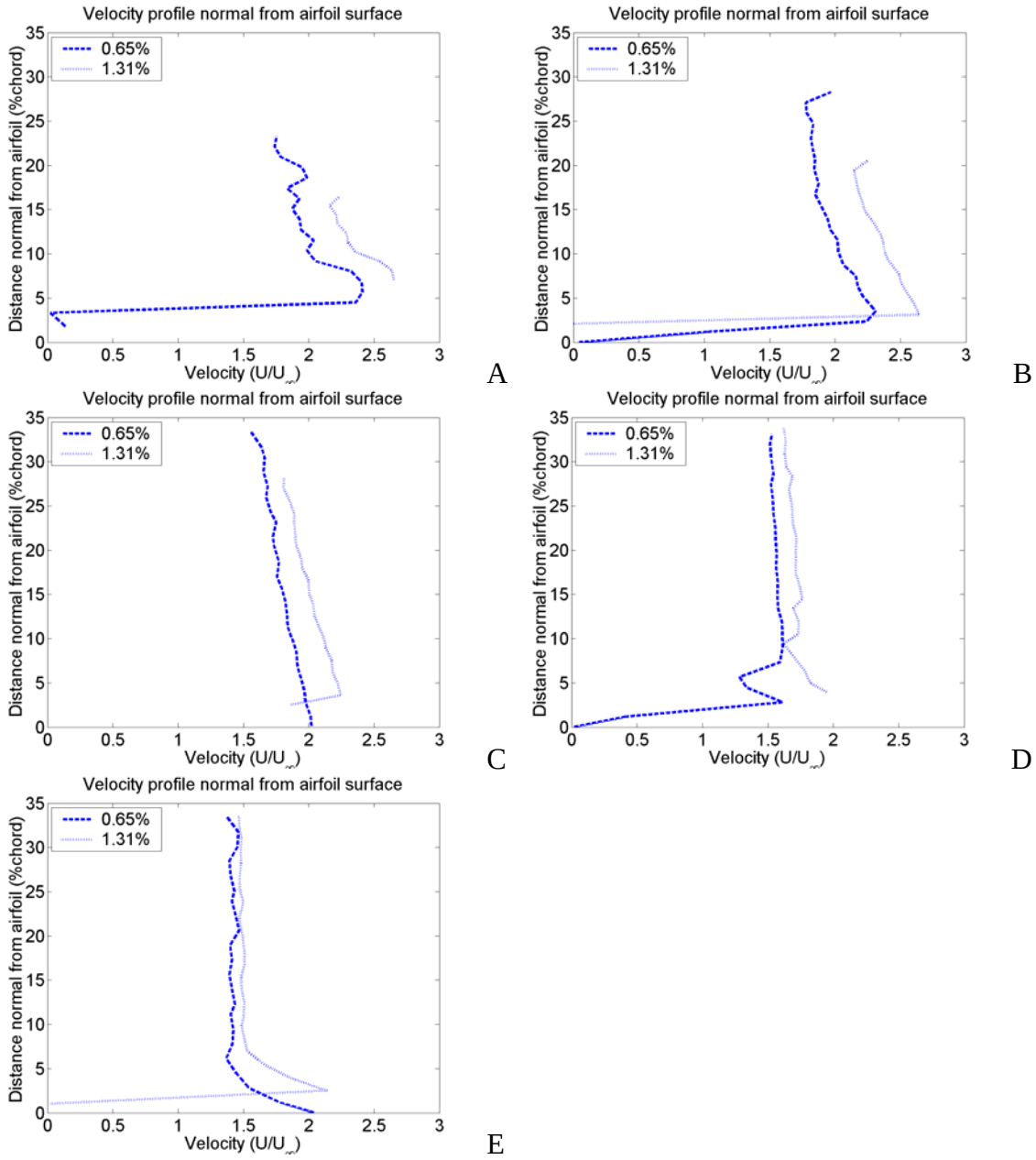

Figure 4-15. Velocity profiles of CFJ0025-065-196 and CFJ 0025-131-196 at 30 degree AOA and various chord locations, A) 5% B) 15% C) 30% D) 50% E) 75%

Figure 4-17 is a group of velocity profiles comparing the flow over the CFJ0025-065-196 airfoil at different angles of attack. Figure 4-18 is all of the profiles grouped together so the flow trend is more visible. It can be seen the greater the angle of attack the higher the velocity of air over the airfoil.

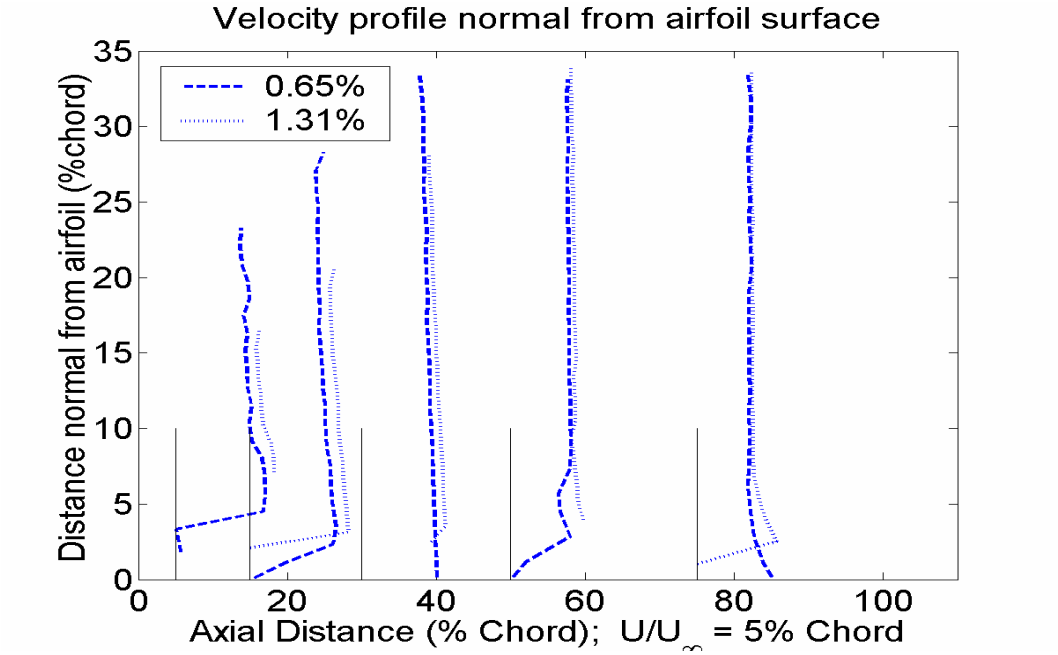

Figure 4-16. Velocity profiles of CFJ0025-065-196 and CFJ0025-131-196 combined into single graph (30 degree AOA)

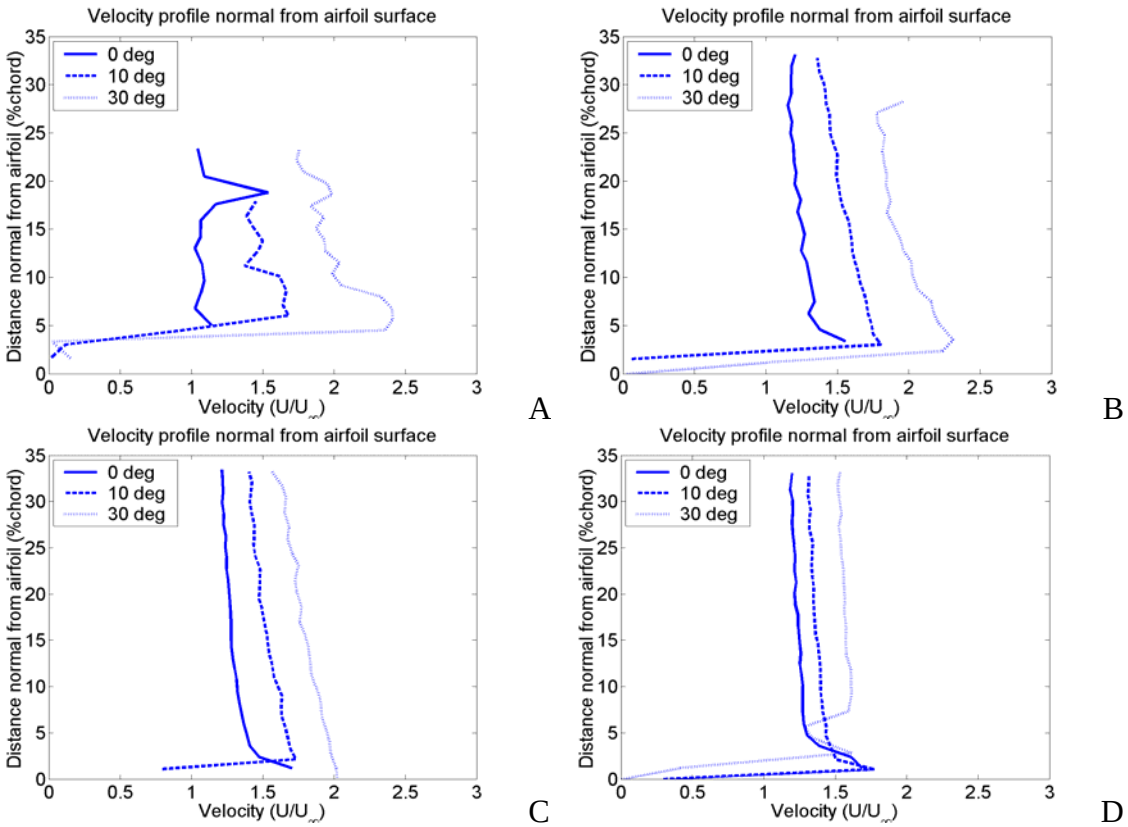

Figure 4-17. Velocity profiles of CFJ0025-065-196 at various AOA and chord locations, A) 5% B) 15% C) 30% D) 50% E) 75% F) 100%

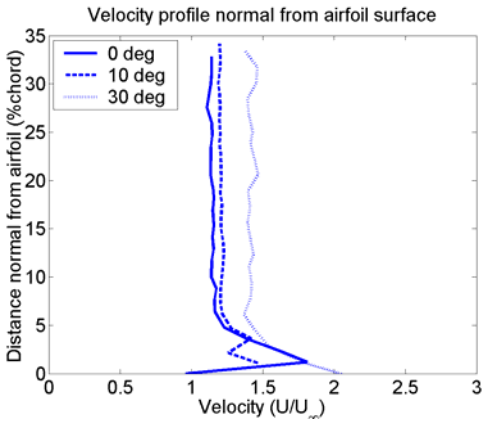

E

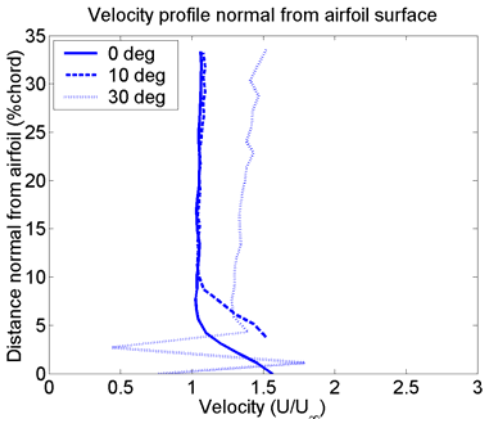

F

Figure 4-17. Continued

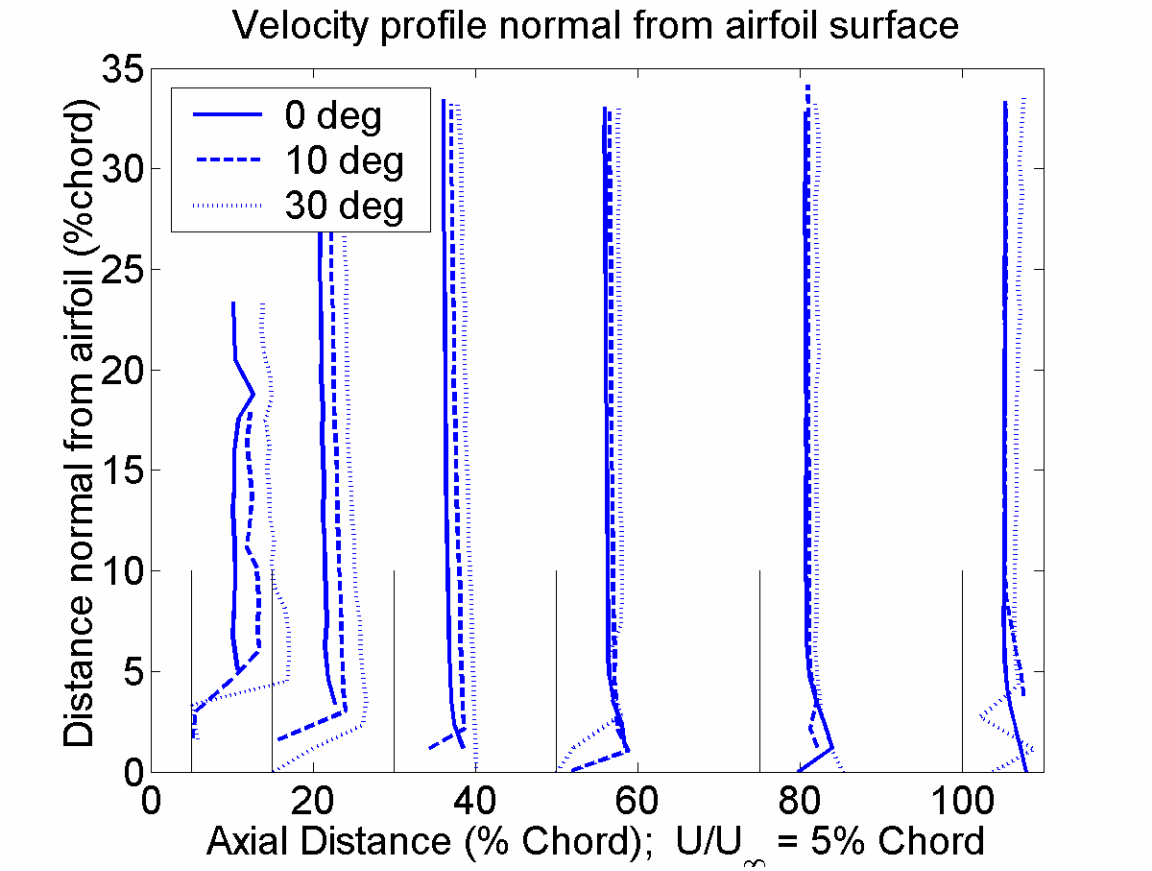

Figure 4-18. Velocity profiles of CFJ0025-065-196 at various AOA combined into single graph

Figure 4-19 is a group of velocity profiles comparing the flow over the CFJ0025-131-196 airfoil at different angles of attack. Figure 4-20 is all of the profiles grouped

together so the flow trend is more visible. It can be seen the greater the angle of attack the higher the velocity of air over the airfoil.

For both the CFJ0025-065-196 and the CFJ0025-131-196 airfoils, the velocities on the fore half of the airfoil are much different than the velocities on the aft half as the angle of attack is increased. The non-dimensional velocities at 15% chord length are very spread, ranging from about 1.3-2.3 and 1.5-2.5 for the CFJ0025-065-196 and CFJ0025-131-196 respectively. The range becomes smaller towards the trailing edge were it is about 1-1.4 for the CFJ0025-065-196 airfoil and is 1.2 for the CFJ0025-131-196 airfoil.

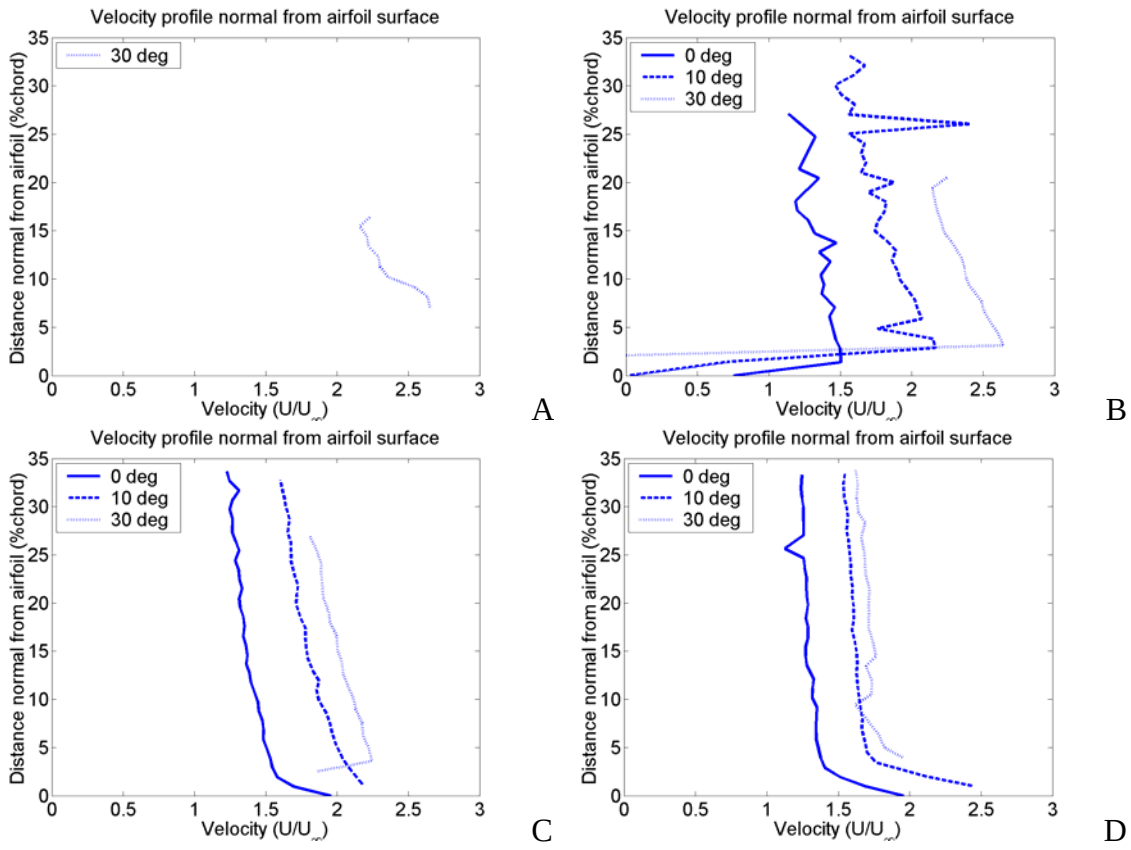

Figure 4-19. Velocity profiles of CFJ0025-131-196 at various AOA and chord locations, A) 5% B) 15% C) 30% D) 50% E) 75% F) 100%

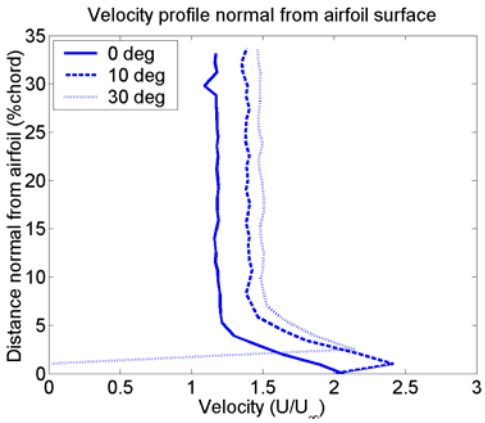

E

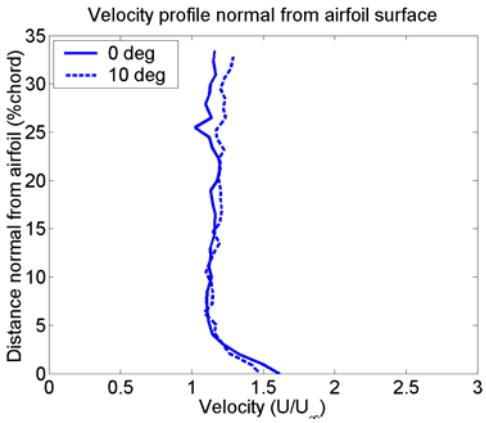

F

Figure 4-19. Continued

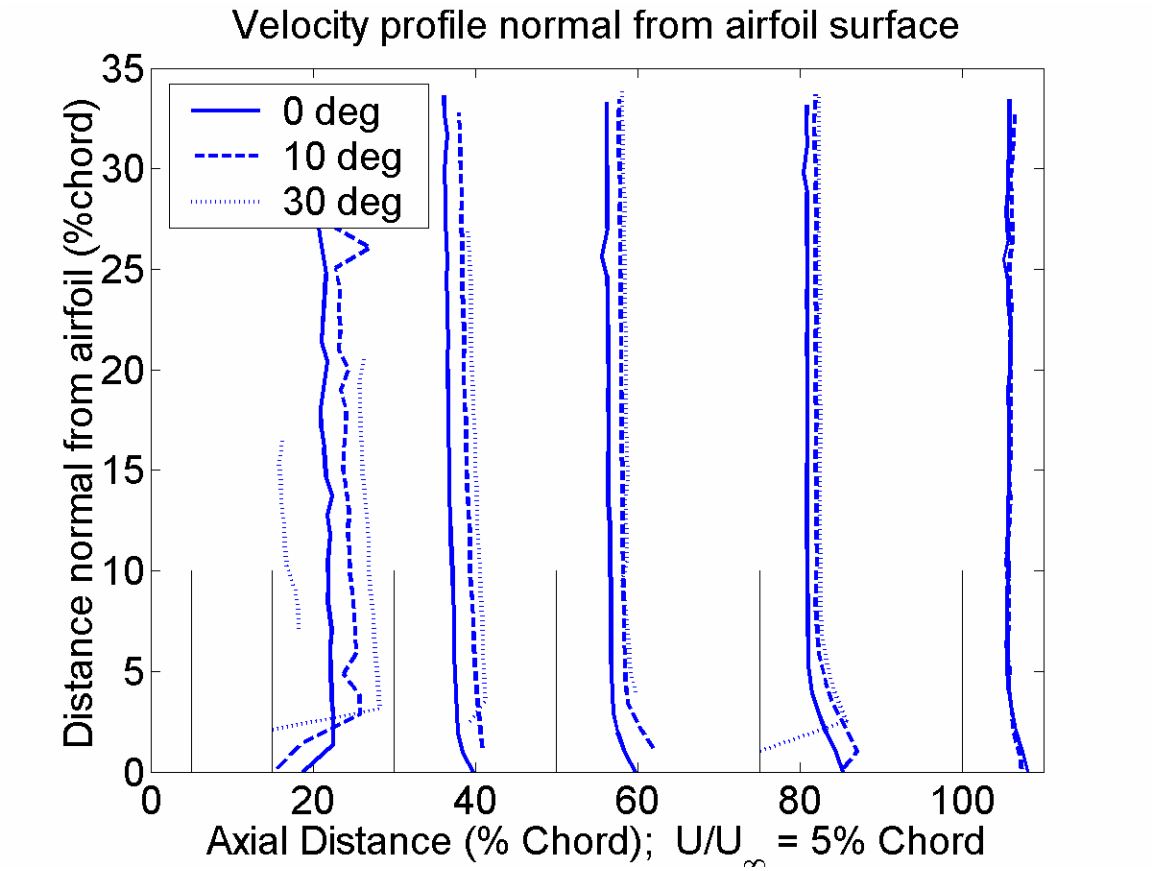

Figure 4-20. Velocity profiles of CFJ0025-131-196 at various AOA combined into single graph.

Another important piece of information that was taken from the PIV data was from the wake images. The NACA 0025 had a wake deficit. The CFJ airfoils on the other hand had a wake surplus. Figures 4-21 and 4-22 show the differences in the wakes at 0

and 10 degrees angle of attack, respectively, for all three airfoil configurations. The wake images were taken approximately one chord length downstream of the airfoil. Again, there was no net mass being injected into the flow. The wake surplus was a result of the momentum being added to the flow.

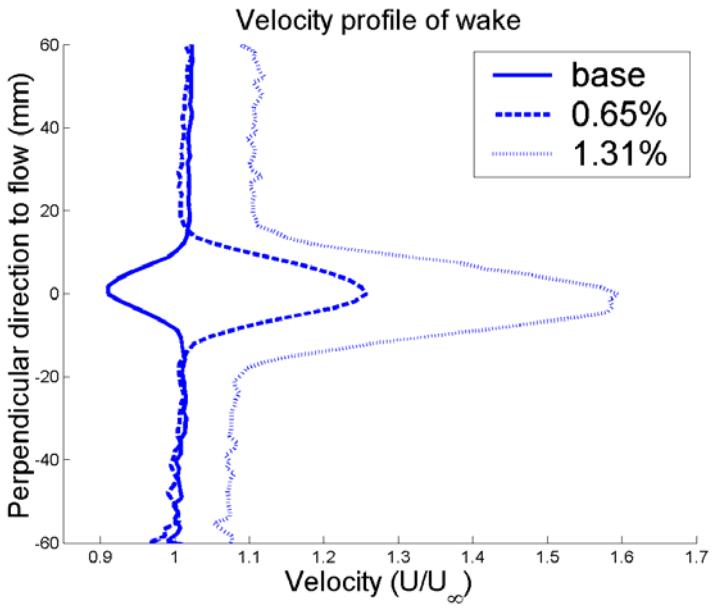

Figure 4-21. Wake profiles of three different airfoil configurations at 0 deg AOA

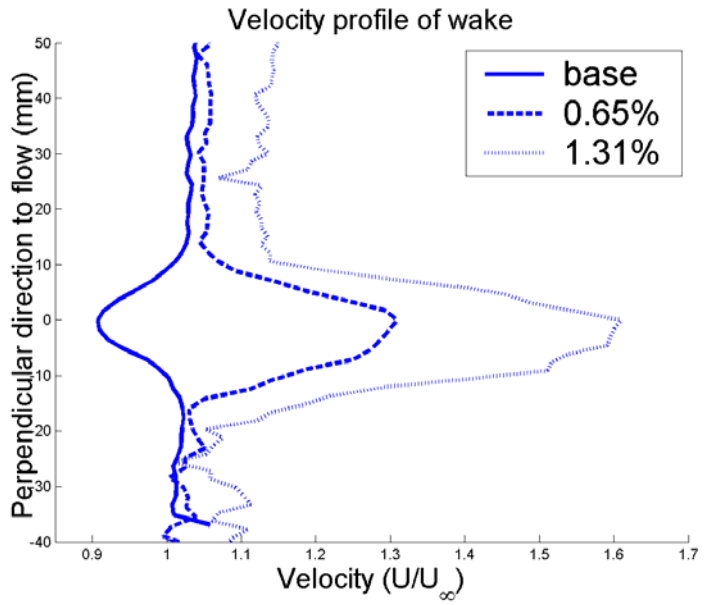

Figure 4-22. Wake profiles of three different airfoil configurations at 10 deg AOA

A velocity profile of the wake was also taken at 30 degrees for the two airfoils utilizing the CFJ flow control technique. It can be seen in figure 4-23 that the wake profile is significantly different. There is no longer a simple wake shape as was seen in the lower angles of attack.

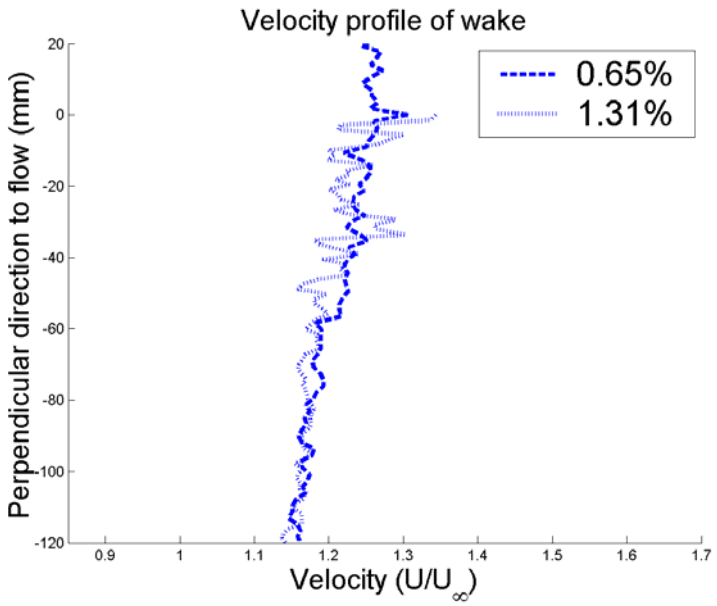

Figure 4-23. Wake profiles of CFJ airfoils at 30 deg AOA

Drag Determination From Wake Measurements

An attempt was made to calculate the drag from the wake profiles with the PIV data. A control volume approach was chosen for this task. The control surfaces encompassed the airfoil and were drawn in such a way as no mass passed through the sides as in figure 4-24. The momentum flux and area exiting the control volume was known from the wake profile. The momentum flux into the control volume was assumed uniform with a velocity equal to the free stream. The inlet area of control volume was adjusted to satisfy the continuity equation; the mass into the control volume had to equal the mass out. The pressure acting on all sides of the control volume was found by equations 4-1 and 4-2. It was assumed T_{total} was constant and equal to 300K.

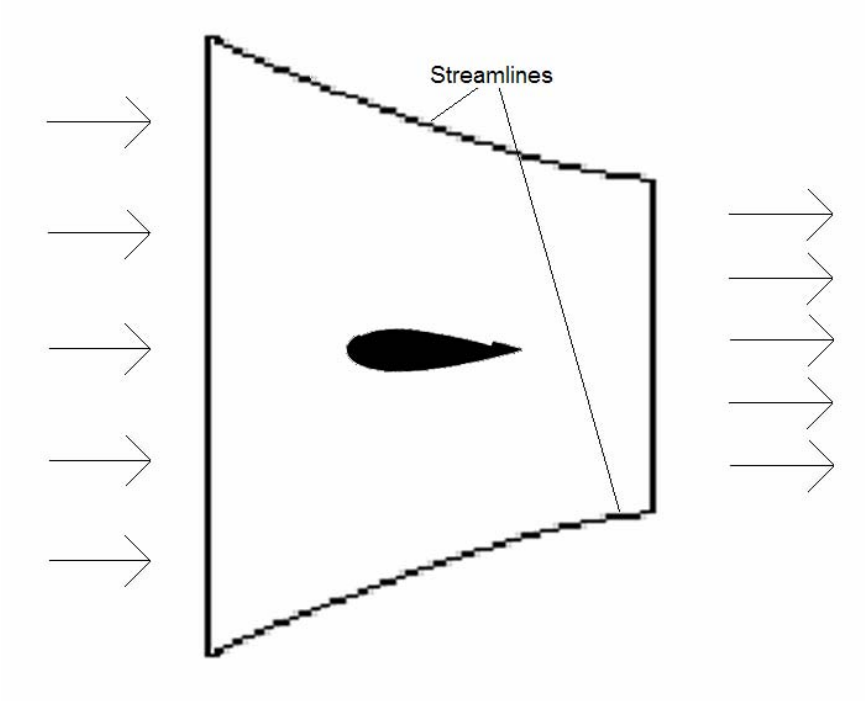

Figure 4-24. Control volume over airfoil

$$T = T_{total} - \frac{\gamma - 1}{2}\frac{V^2}{\gamma R} \qquad \text{Eqn 4-1}$$

$$P = \rho RT \qquad \text{Eqn 4-2}$$

The above approach did not yield valid results. It is thought calculating the pressures acting on the control volume from velocity measurements alone is not enough. Future work will include taking pressure readings along the boundaries of the control volume as well as velocity measurements.

CHAPTER 5
CONCLUSIONS

The research described in this thesis successfully demonstrated how the CFJ airfoil transitioned from CFD modeling to wind tunnel testing. The research proved the high performance capabilities of the CFJ airfoil. It was shown the smaller injection slot airfoil performed better than the larger injection slot airfoil with respect to maximum lift and stall margin. It was also shown the larger injection slot airfoil performed better than the smaller injection slot airfoil with respect to lift for a given angle of attack and drag reduction.

The PIV data revealed evidence of how the stagnation point location moves with varying mass flow rates. The movement of the stagnation point results in different lift and drag characteristics. The PIV data taken was used to make velocity profiles of the CFJ airfoil and compare them to a conventional airfoil. The data also was used to compare velocity profiles of the two different CFJ airfoils used in wind tunnel tests.

Although the research conducted in this thesis was successful, much work lies ahead. The PIV setup will need to be improved to better understand the location and movement of the stagnation point. The instability of the jet also needs to be looked into further as the exact cause is still unknown at this time.

Much optimization still remains for the CFJ airfoil geometry. The geometry of the airfoil was chosen from CFD simulations. Only two different injection slot sizes were tested in the wind tunnel. Many different slot heights should be tried, both for the injection and for the suction. The slot location will also have a significant effect on the

performance of the airfoil. In future work, it is planned to have an injection slot that can be adjusted for both location and height.

The amount of mass injected can be controlled by a number of different means. It is not know which of these is the best method to obtain the peak performance. The mass injected can be controlled by a direct measurement of the mass flow rate. The stagnation pressure of the injection jet or the jet momentum coefficient can also control the mass injected. It might also be beneficial to control the velocity of the injection jet.

An in-depth study of the shear-mixing region would also be advantageous to the success of the CFJ airfoil. It is known the CFJ airfoil suppresses separation and increases lift from the addition of momentum and the induced mixing with the free stream. The mechanics of the turbulent shear layer mixing the free stream and the jet is largely unknown.

Future work also consists of investigating three-dimensional effects of a wing utilizing a CFJ. Work here would include looking at tip effects due to the CFJ. Other items to be looked at include the length the slots should extend towards the wingtips and if there should be any variation is the slot height or location along the wingspan.

APPENDIX A
DETAILED CALIBRATION PROCEDURE

1. Plug in power supply and data acquisition/switch unit
2. Check the power supplies 5V output with the Multimeter to make sure the output is indeed 5V
3. Connect all appropriate connections
    a. Connect nine pin to BNC breakout box
    b. Connect power supply to BNC breakout box
    c. Connect BNC cables from breakout box to appropriate connections on data acquisition/switch unit
    d. Connect data acquisition/switch unit to computer
4. If this calibration has already been preformed and the experimentalist wants only to check the accuracy of the calibration or reading, go to step 17
5. Rigidly attach balance cylinder to fixed object such as an optical table
6. Attach metal calibration bar to end of cylinder where the airfoil attaches
7. Rotate the cylinder until it reaches an appropriate angle (an appropriate angle is one in which the normal and axial forces are in the range of expected experimental normal and axial forces)
8. Measure the angle with an inclinometer
9. Open up Labview VI previously made for balance calibration and enter necessary information
    a. Angle
    b. Run number
    c. Number of samples to take
    d. Data folder to save information to
10. Press the tare button. This will nullify any voltage currently being read.
11. Take a reading at zero load
12. Hang a 1kg mass from the hole in the metal bar, take care to steady any oscillatory motion of the mass
13. Increase the mass to 1kg in the Labview program
14. Take a reading at this load condition
15. Increase the mass hanging from the hole in the metal bar 1kg at a time until the maximum expected experimental force is achieved. Be sure to take readings for each increment and change the mass in the Labview program accordingly.
16. Plot the voltage verse force to come up with an initial calibration curve for the normal and axial force
17. Place the fully assembled airfoil into the wind tunnel suction side down
18. Press the tare button in the Labview program written for wind tunnel testing
19. Place a 1kg weight in the center of the span of the airfoil
20. Record the force the program is reading for lift

21. Repeat steps 19 and 20 increasing the weight until it exceeds the maximum force expected
22. Turn the airfoil so the LE is pointing straight up
23. Place a 1kg weight in the center of the span of the airfoil for this orientation too
24. Record the force the program is reading for drag
25. Plot the known load verse indicated load for both lift and drag
26. The slopes of the curves are the corrections needed for the latex tubes. Adjust the initial calibration accordingly.
27. Check to see if the airfoil is now calibrated correctly by placing known weights on the center span making sure the program is reading the correct force

APPENDIX B
LIST OF INSTRUMENTATION AND EQUIPMENT

Instrumentation Used for Wind Tunnel Experiment
Pressure Measurements:
Heise ST-2H SN 50520
Model HQS-1 Range 0-15" H2O SN HQS-15557
Model HQS-2 Range 0-30 psia SN HQS-18121

Heise ST-2H SN 50841
Model HQS-1 Range 0-50" H2O SN HQS-17943
Model HQS-2 Range 0-250 psia SN HQS-18120

Druck DPI 145 Multifunction pressure indicator SN 0721/98-08

Temperature Measurements:
National Instruments SCXI-1000 Mainframe SN 002894
National Instruments SCXI-1303 SN A18FE3

Force Measurements:
Tektronix PS280 DC Power Supply SN PS280 TW58011

Hewlett Packard 34970A Data Acquisition/Switch Unit
Agilent 34901A 20-channel armature multiplexer

Ninepin-to-BNC breakout box

Power to control valve:
Tektronix PS280 DC Power Supply SN PS280 TW11432

National Instruments SCB-68 Breakout Box SN BAD24C

PIV Measurements:
TSI Power View Camera Model 630151 SN 14250

TSI Laser Pulse Synchronizer Model 610032 SN 220

Equipment Used for Wind Tunnel Experiment

Aerolab Educational Wind tunnel
- Open circuit
- 12" x 12" test section, 24" long
- 0-145 mph capability from 10 hp drive fan

Measurement Group, Inc.
- Type EA-13-125MK-120 strain gauge
- Type EA-06-125TK-350 shear gauge

Applied with M-Line products:
- CSM-1A degresser
- M-Prep Conditioner A
- M-Prep Neutralizer 5A
- M-Bond 200
- Gauze sponges
- Cotton swabs
- PCT-2A cellophane tape
- M-Coat A
- Rosin solvent
- 400-grit sand paper

T type thermocouple from Omega

K type thermocouple from Omega

Quincy Compressor Division, Model QSI-1000ANA3HP SN 3N93685H

Welsh Vacuum Pump, Model 1398 SN 083D

Heraeus Vacuum Pump, Type E35 Fabrication# 03501409

Fisher 667 Control Valve SN 15940894

LeMaitre G150 Fog Machine SN G15C00280

Computers and Software Used for Wind Tunnel Experiment

Lift and drag measurements:

AMD Athlon XP 1800+ Microsoft Windows XP Professional

Labview 6.1

PIV measurements:

AMD Athlon XP 2500+ Microsoft Windows 2000

Insight

APPENDIX C
DETAILED AIRFOIL ASSEMBLY PROCEDURE

1. Attach L-brackets to optical table with 1/4-20 allen screws and washers
2. Attach rear canister plate and sting collet to L-brackets with 1/4-20 screws
3. Attach sting cylinder to sting cylinder clamp
    a. Orient the clamp so the open side will point towards the TE of the airfoil
    b. Clamp should be flush with the end of the cylinder
    c. Attach clamp directly to cylinder using M2/6 screws
    d. Tighten clamp around cylinder with M3/12 screw
4. Attach sting clamp/cylinder assembly to injection side airfoil endplate with M4/18 screws
5. Attach airfoil to injection side assembly (cylinder, clamp, endplate)
    a. Clamp will fit inside airfoil with clamping section facing TE
    b. Attach airfoil first with M4/40 screws then M2/20
    c. Tighten all screws firmly
6. Attach Kiel stagnation pressure probe to suction side airfoil endplate
    a. Thread the mounting chuck into the external side of the endplate
    b. Feed the probe from the internal side of the endplate through the mounting chuck
    c. Tighten the mounting chuck compression fitting onto the probe
    d. Make sure the probe faces the normal direction to the flow
    e. Lock in place
7. Make sure Duocel aluminum foam is in airfoil, if not place in now
8. Attach suction side airfoil endplate to the airfoil assembly
    a. Attach airfoil first with M4/40 screws then M2/20
    b. Tighten all screws firmly
9. Slide the tunnel wall circular plate onto the cylinder
    a. The tunnel wall should have the inside of the wall facing the airfoil
    b. Being careful to feed the strain gauge wires through the center of the wall
    c. Being careful not to damage the strain gauges or their solder connections
10. Slide the cylinder into the collet that is attached to the optical table
    a. Make sure collet is in fully open position
    b. Being careful not to jostle tunnel wall and strain gauges
    c. Make sure the o-ring in the center of the endplate stays in place
    d. Push the cylinder into the collet until it aligns with previously marked location (this ensures proper alignment in tunnel)
    e. Tighten collet to lock cylinder in place
11. Remove airfoil assembly from optical table
12. Attach endplate to collet with 1/4-20 screws
13. Attach strain gauge nine pin connection to adapter fixed to endplate
14. Attach the canister to the endplate/collet assembly

   a. Slide the canister over the endplate/collet assembly
   b. Line up the bolt holes in the canister with the bolts of the tunnel wall
   c. Slide the canister up until it touches the endplate
   d. Make sure not to pinch any strain gauge wires
   e. Tighten the endplate with the canister with 1/4-20 allen screws
   f. Tighten the tunnel wall to the canister
15. Attach entire assembly to the wind tunnel
   a. Pass the assembly through the side of tunnel opposite the side the assemble is to be fixed to
   b. Place the assembly such that the tunnel wall circular plate fits into the circular cut out in the tunnel
   c. Attach optical clamps on the outside of the tunnel wall to hold the assembly in place
16. Replace Plexiglas tunnel wall with Plexiglas box tunnel wall
17. Attach internal box suction manifold to circular box wall and external box suction manifold
   a. Line up the box external suction manifold on the outside of the box circular plate with the oval opening
   b. Line up the box internal suction manifold on the outside of the box circular plate with the oval opening
   c. Make sure the internal and external manifolds are lined up with only the box circular plate between them
   d. Bolt these three components together with four 1/4-20 nuts and bolts
18. Prepare latex tubes to be attached to airfoil suction manifold
   a. Stretch the tubes over the three receiver ports on the suction manifold
   b. Fix in place with hose clamps
   c. Stretch the tubes over the three receiver ports on the internal box suction manifold
   d. Fix in place with hose clamps
   e. Check spacing of metal rings inside the tubes, move as necessary
   f. Glue into place and let glue dry
19. Attach suction manifold to the airfoil already in wind tunnel
   a. Slide airfoil suction manifold through the hole in the suction side tunnel wall circular plate
   b. Place the tunnel wall circular plate to the suction side of the airfoil such that the Kiel probe assembly protrudes through the small hole in the circular plate
   c. Also the suction manifold should be lined up with the suction slot on the airfoil endplate
   d. Screw the suction manifold to the suction side airfoil endplate with M4/20 screws
20. Secure the Plexiglas box side of the wind tunnel
   a. The suction side circular tunnel wall will fit into the recess of the tunnel side door when the box is closed
   b. The suction side circular box wall will fit into the recess of the box when the side door is closed

    c. Lock the side door with the lever attachment on the wind tunnel
    d. Lock the box wall and tunnel wall in place with optical brackets
21. Attach static pressure probe to suction manifold
    a. Feed the static probe through the hole on the bottom of the airfoil suction manifold
    b. Slide mounting chuck over the probe and into the hole
    c. Thread the mounting chuck into the hole and tighten the mounting chuck compression fitting
    d. Be sure to face the probe normal to flow direction
    e. Lock in place
22. Attach probes to appropriate connections inside of box
    a. Kiel probe to stagnation pressure tube
    b. Static suction probe to static pressure tube
    c. Injection thermocouple to injection thermocouple wires
    d. Suction thermocouple to suction thermocouple wires
23. Place the lid on the box and screw down with M2/10 screws
24. Replace ceiling and floor of wind tunnel if removed
25. Attach injection hose to hollow cylinder and secure with hose clamp
26. Attach PVC suction pipe to external manifold and wrap connection with duct tape

APPENDIX D
DETAILED WINDTUNNEL ASSEMBLY PROCEDURE

1. Turn on vacuum pump and begin pulling vacuum
    a. Close all valves open to the atmosphere
    b. Open all valves to the vacuum tanks both rooms
    c. Turn on vacuum breaker
    d. Go to pump located outside of MAE-A
    e. Close valves directly after pump
    f. Push start buttons on wall behind pumps
    g. Open valve after pump a quarter of the way (opening the this valve more than this will result in lots of smoke from the oil becoming too hot)
    h. Fully open valves to Room 119 and Room 125
2. Start compressor
    a. Check with other labs to see if they are using the compressor
    b. Close valve coming out of the compressor house
    c. Fill out the log in the compressor house
    d. Turn on main power supply
    e. Make sure stop button is pulled out
    f. Push start button (NEED HEARING PROTECTION)
    g. Watch for a couple of minutes to see if any warning lights come on
    h. Open valve coming out of the compressor house
3. Assemble and mount airfoil as described in assembly procedure
4. Connect different probes to appropriate transducers
    a. Thermocouples
    b. Pressure transducers
    c. Strain gauges
5. Turn on all instrumentation and computer
    a. Heise x 2
    b. SCXI
    c. Druck
    d. Power supply for strain gauges
    e. HP switch unit
6. Start Labview program made for this experiment
7. Make sure all probes are reading correctly in Labview VI (Tare if needed)
8. Set zero degree angle of attack
    a. Make sure the airfoil is securely in place and the circular wind tunnel plate is flush with the tunnel wall
    b. Adjust the airfoil so the TE is 6" from the wind tunnel floor
    c. Mark circular wind tunnel plate to indicate zero degrees angle of attack
9. Rotate airfoil to desired angle of attack
    a. Loosen optical clamps on the circular tunnel walls and circular box wall

   b. Rotate all three in unison until reached desired angle of attack
   c. Tighten all three with optical clamps
10. Enter necessary information into program
   a. Angle of attack
   b. Ambient pressure
   c. Ambient temperature
   d. Area of injection jet
11. Turn on wind tunnel
   a. Turn on wind tunnel breaker
   b. Push forward run button on wind tunnel
   c. Switch to Front Panel control on wind tunnel display
   d. Rotate Fan Speed Control until desired velocity is reached
12. Start air injection
   a. Make sure switch above wind tunnel is turned in the direction to measure injection mass flow rate
   b. Let pressure reach 200 psi in tanks
   c. Make sure control valve is closed
   d. Fully open valve downstream of control valve
   e. Open valve upstream of control valve a quarter way
   f. Slowly open control valve until close to the desired mass flow rate
   g. Slightly adjust the valve upstream of the control valve to fine tune the mass flow rate
13. Dial in suction mass flow rate
   a. Make sure the tank pressure is always reading below 15 in Hg through out the run, this ensures the flow is choked at the gate valve creating a constant mass flow rate, wait until the pressure lowers if necessary
   b. Once the injection mass flow rate is desirable and steady turn the switch above the wind tunnel to measure the suction mass flow rate
   c. Open the gate valve next to the vacuum tanks slightly
   d. Fully and quickly open ball valve above the gate valve to start suction (NEED HEARING PROTECTION)
   e. The mass flow rate then needs to be adjusted to the desired rate, this can be done by:
      i. Short bursts of vacuum (just long enough to achieve a reading), then adjust the gate valve with the vacuum is off and repeat
      ii. Continuous vacuum while adjusting the gate valve
   f. Refer to a. if the desired mass flow is not achieved after 15 seconds of vacuum
14. Only continue after the suction mass flow rate is desirable
15. Start air suction and sampling
   a. Make sure the tank pressure is always reading below 15 in Hg through out the run, this ensures the flow is choked at the gate valve creating a constant mass flow rate, wait until the pressure lowers if necessary
   b. Double check that all probe measurements are working correctly
   c. Turn switch above wind tunnel to measure mass flow of injection
   d. Make sure injection flow rate is still desirable

e. Make sure Start Sampling and Stop Sampling buttons are not lit up. If they are click on the button to turn off
f. Push Start Sampling button in VI
g. Fully and quickly open ball valve above the gate valve to start suction (NEED HEARING PROTECTION)
h. After 5 seconds, turn valve above wind tunnel to measure injection mass flow rate
i. Continue to sample for desired time, keep in mind a.
j. Push Stop Sampling button to save data

APPENDIX E
PIV IMAGES

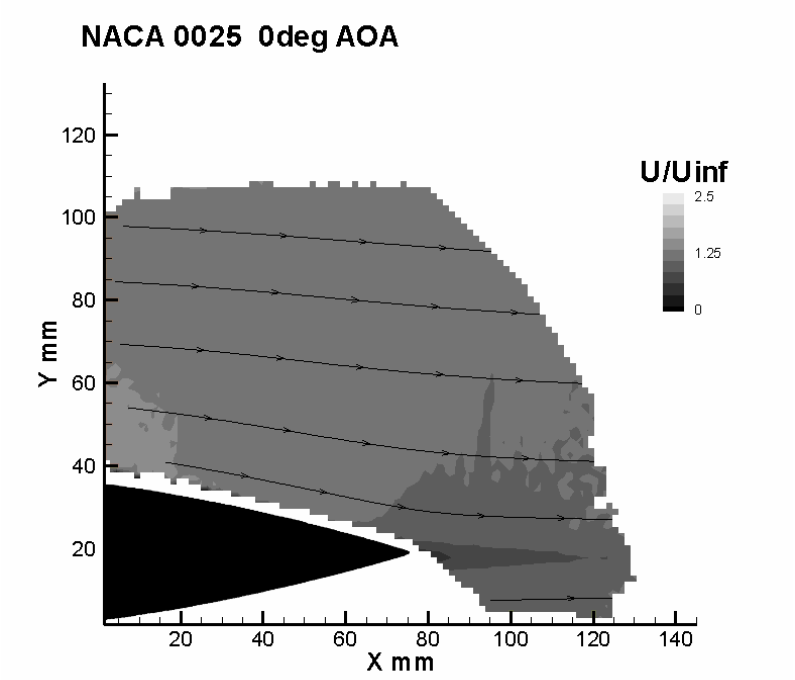

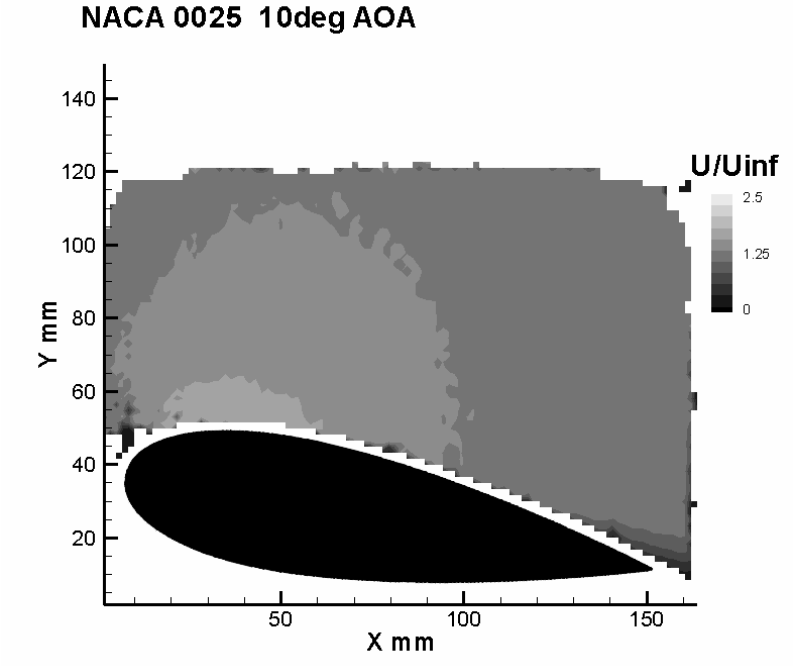

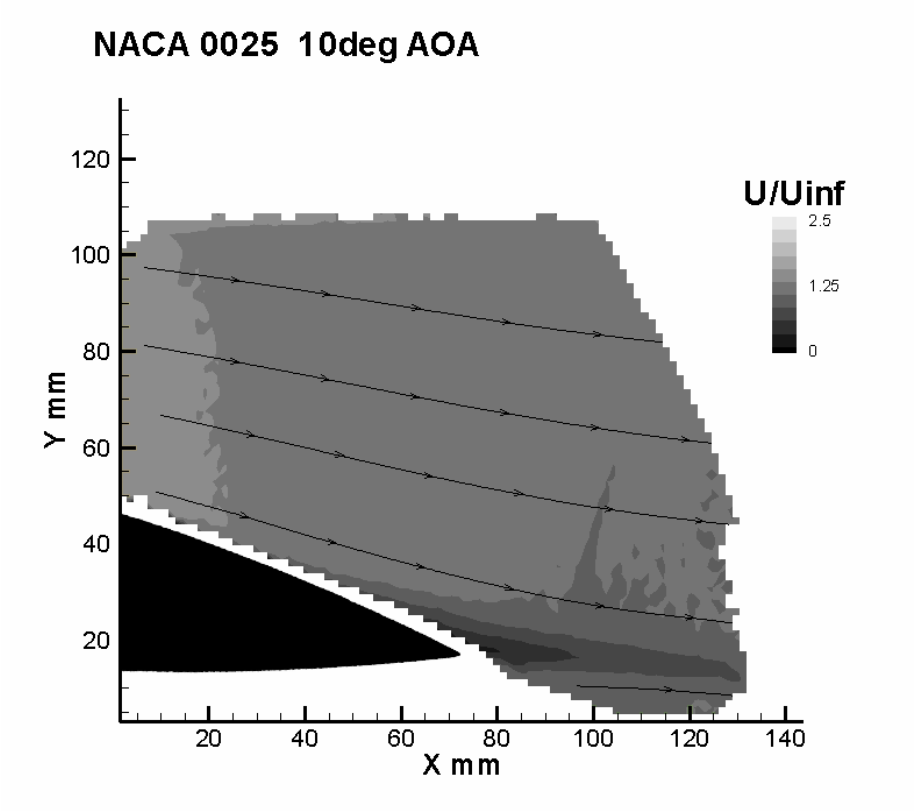
NACA 0025 10deg AOA
U/Uinf
2.5
1.25
0
Y mm
120
100
80
60
40
20
20
40
60
80
100
120
140
X mm

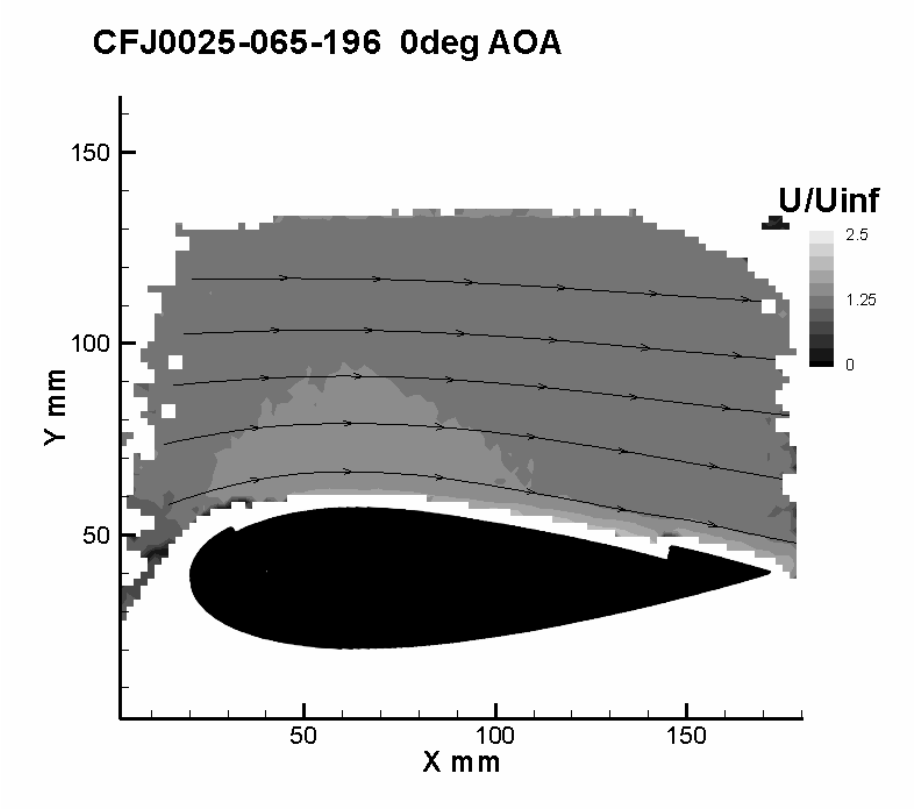
CFJ0025-065-196 0deg AOA
U/Uinf
2.5
1.25
0
Y mm
150
100
50
50
100
150
X mm

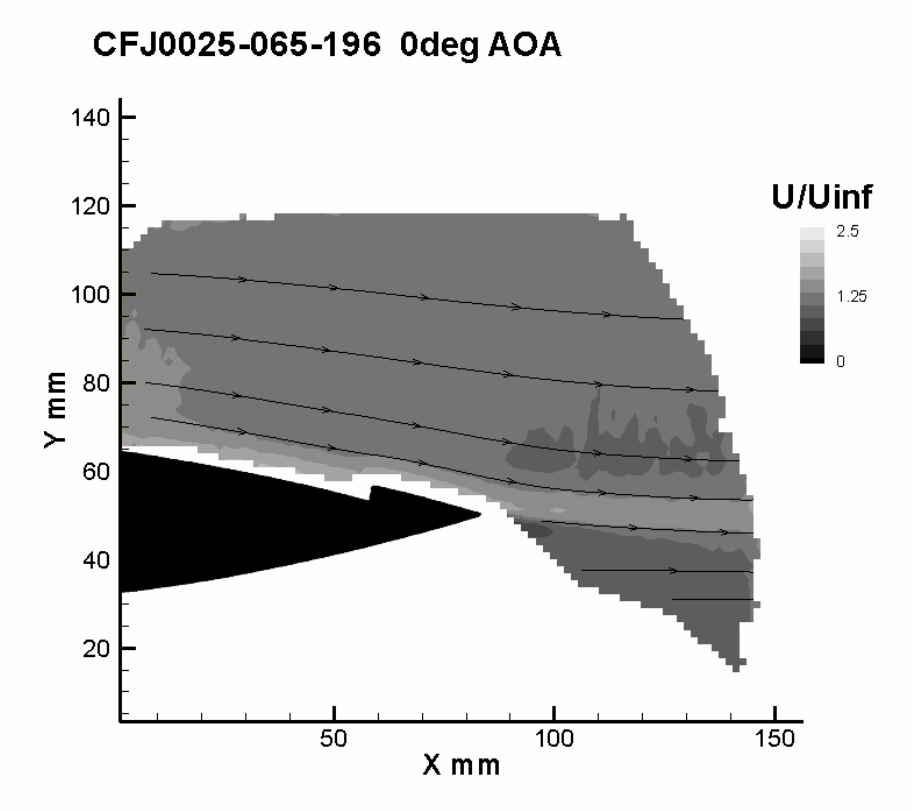
CFJ0025-065-196 0deg AOA
U/Uinf
2.5
1.25
0
Y mm
140
120
100
80
60
40
20
50
100
150
X mm

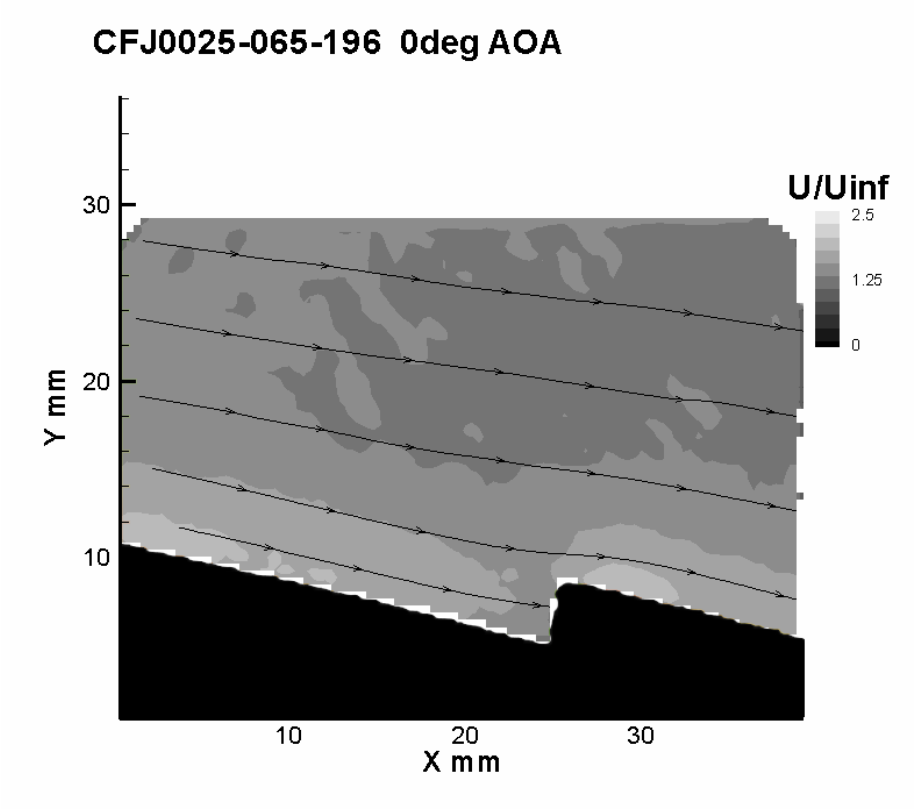
CFJ0025-065-196 0deg AOA
U/Uinf
2.5
1.25
0
Y mm
30
20
10
10
20
30
X mm

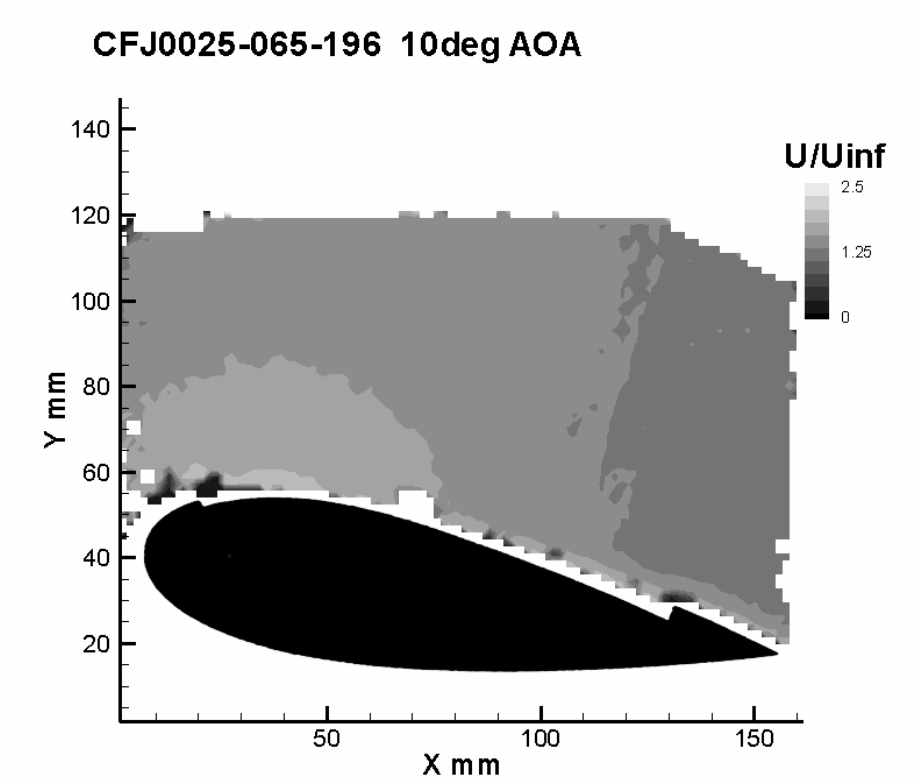
CFJ0025-065-196 10deg AOA
U/Uinf
2.5
1.25
0
Y mm
X mm
140
120
100
80
60
40
20
50
100
150

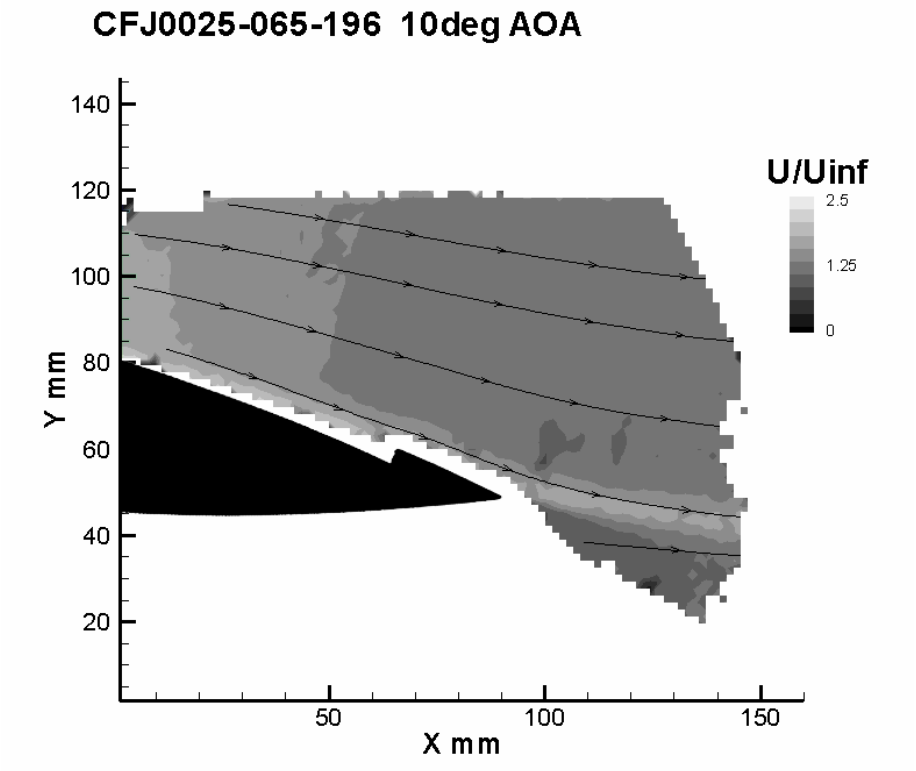
CFJ0025-065-196 10deg AOA
U/Uinf
2.5
1.25
0
Y mm
X mm
140
120
100
80
60
40
20
50
100
150

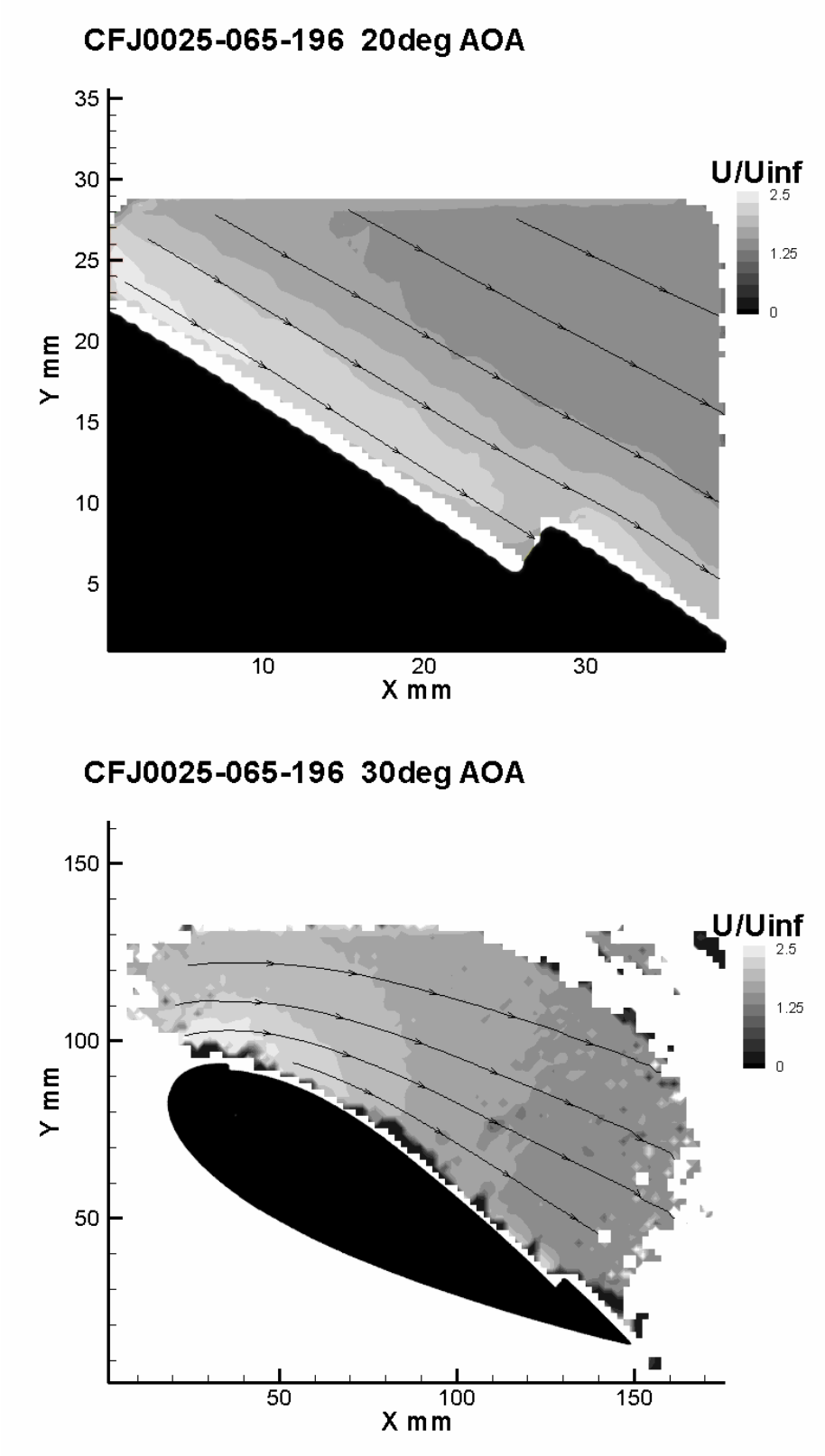
CFJ0025-065-196 20deg AOA
U/Uinf
2.5
1.25
0
Y mm
X mm
35
30
25
20
15
10
5
10
20
30
CFJ0025-065-196 30deg AOA
U/Uinf
2.5
1.25
0
Y mm
X mm
150
100
50
50
100
150

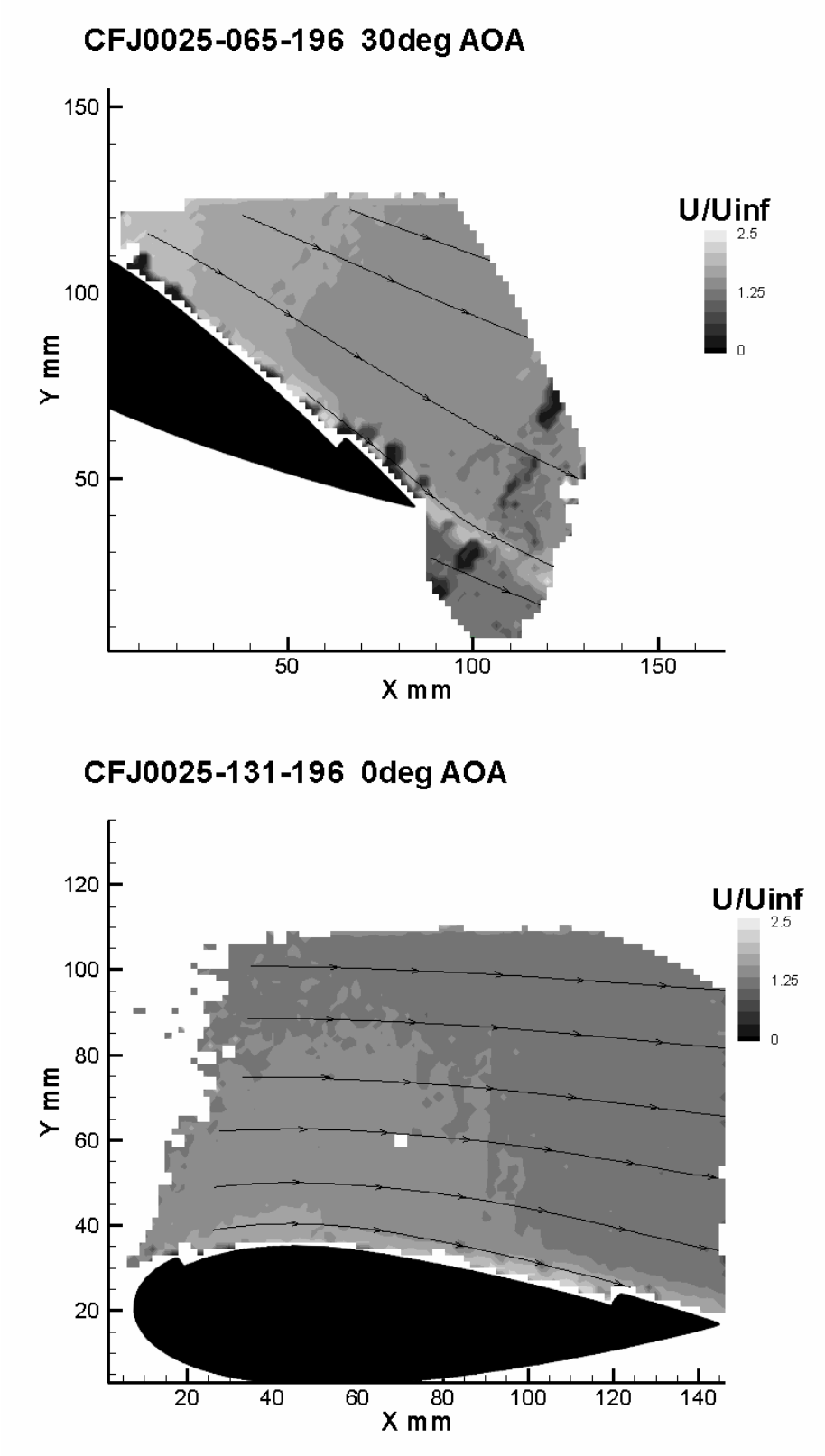
CFJ0025-065-196 30deg AOA
U/Uinf
2.5
1.25
0
Y mm
X mm
150
100
50
50
100
150
CFJ0025-131-196 0deg AOA
U/Uinf
2.5
1.25
0
Y mm
X mm
120
100
80
60
40
20
20
40
60
80
100
120
140

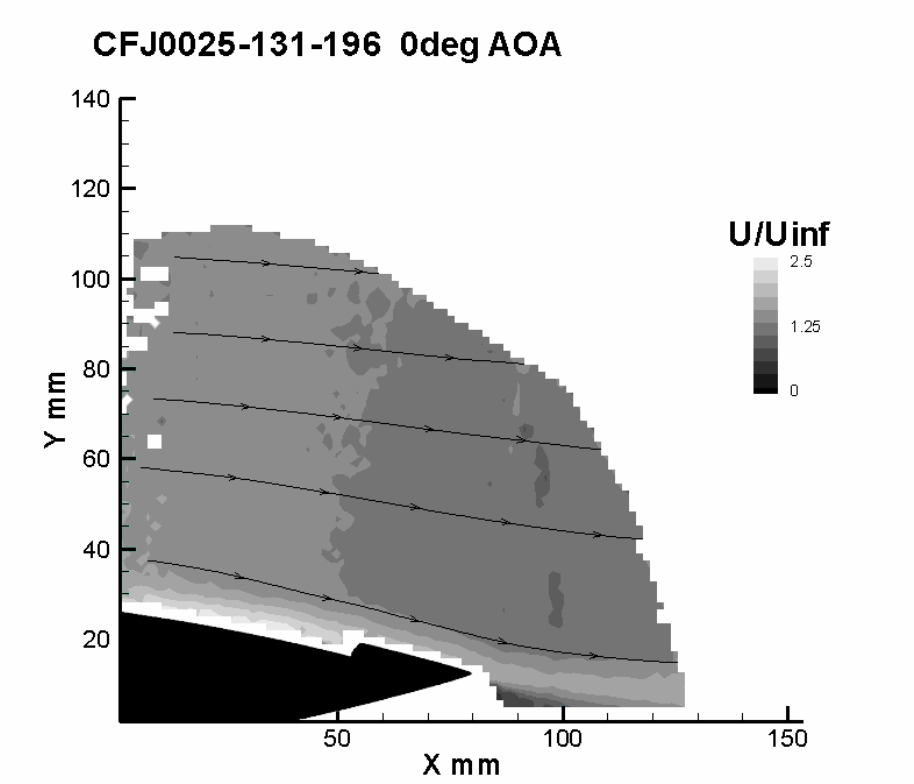
CFJ0025-131-196 0deg AOA
U/Uinf
2.5
1.25
0
Y mm
X mm
140
120
100
80
60
40
20
50
100
150

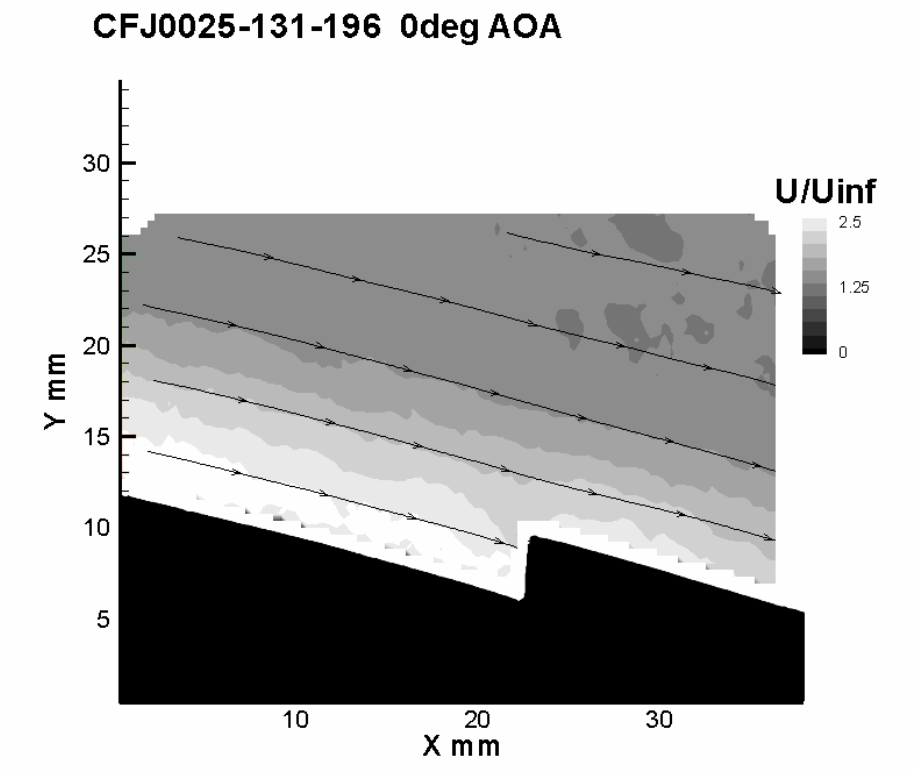
CFJ0025-131-196 0deg AOA
U/Uinf
2.5
1.25
0
Y mm
X mm
30
25
20
15
10
5
10
20
30

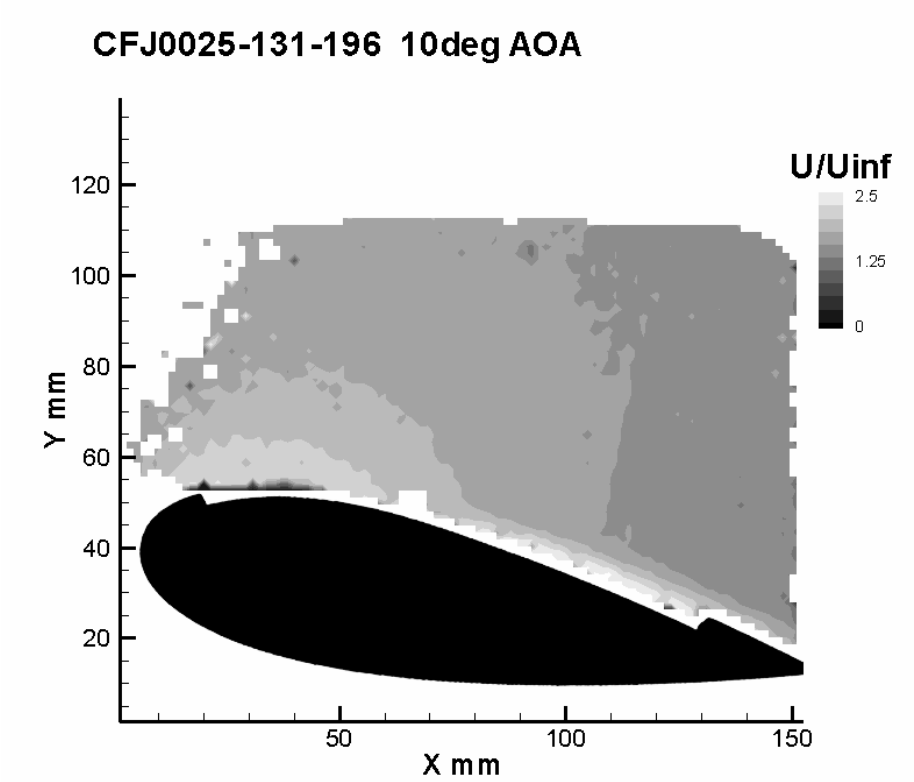
CFJ0025-131-196 10deg AOA
U/Uinf
2.5
1.25
0
120
100
80
60
40
20
Y mm
50
100
150
X mm

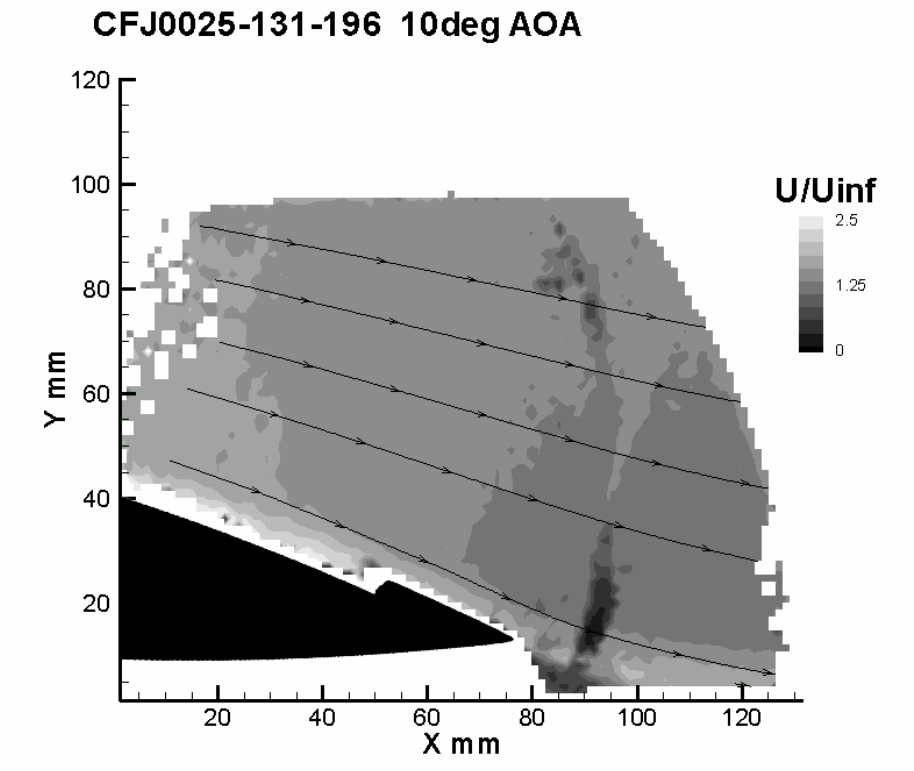
CFJ0025-131-196 10deg AOA
U/Uinf
2.5
1.25
0
120
100
80
60
40
20
Y mm
20
40
60
80
100
120
X mm

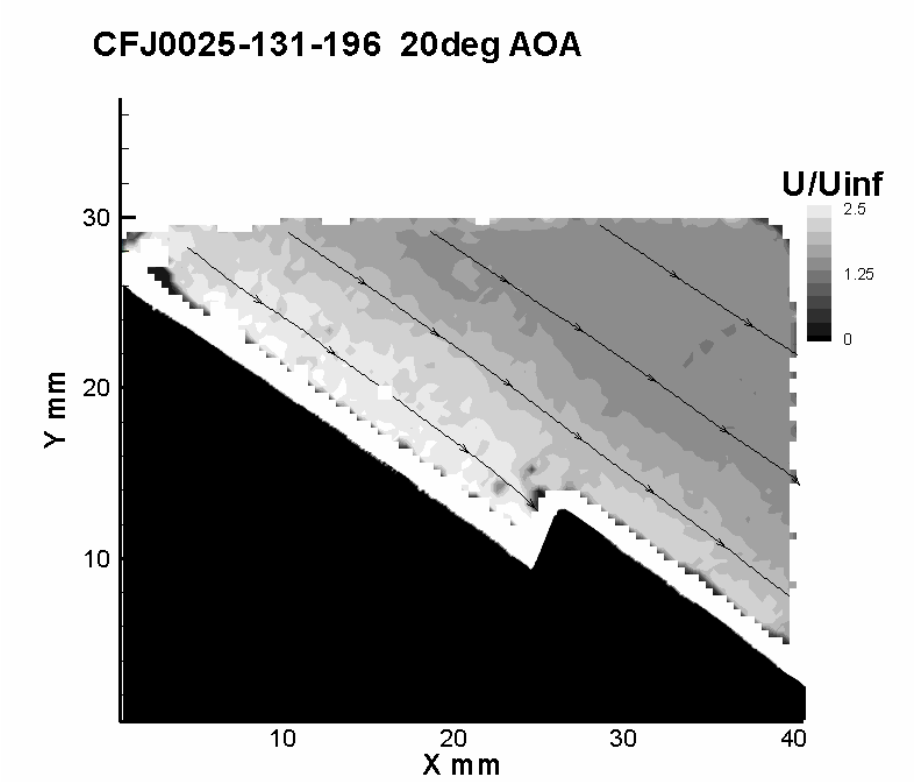
CFJ0025-131-196 20deg AOA
U/Uinf
2.5
1.25
0
Y mm
30
20
10
10
20
30
40
X mm

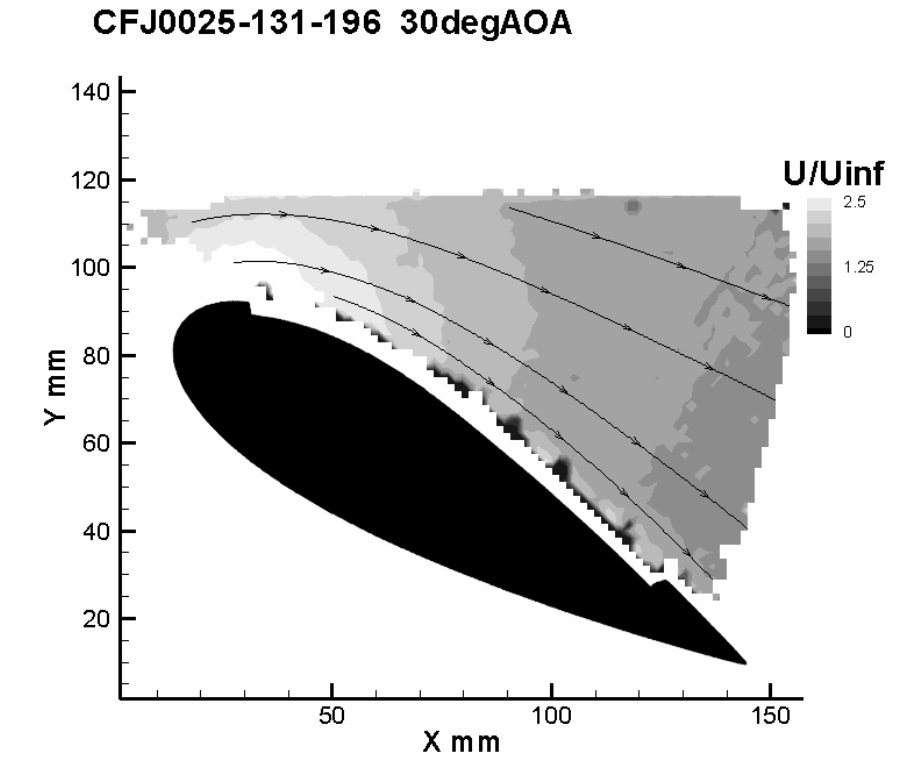
CFJ0025-131-196 30degAOA
U/Uinf
2.5
1.25
0
Y mm
140
120
100
80
60
40
20
50
100
150
X mm

LIST OF REFERENCES

1. Zha, G.-C. and Paxton C., "A Novel Airfoil Circulation Augment Flow Control Method Using Co-Flow Jet." AIAA Paper 2004-2208, 2nd AIAA Flow Control Conference, Portland, Oregon, June 28-1, 2004.

2. Modi V., Fernando M., and Yokomizo T., "Drag Reduction of Bluff Bodies Through Moving Surface Boundary Layer Control." AIAA Paper No. 1990-298, 28th Aerospace Sciences Meeting, Reno, Nevada, January 8-11, 1990.

3. Wood N., Robert L., and Celik Z., "Control of Asymmetric Vortical Flows over Delta Wings at High Angle of Attack," *Journal of Aircraft*, vol. 27, pp. 429-435, 1990.

4. Wood N. and Robert L., "Control of Vortical Lift on Delta Wings by Tangential Leading-Edge Blowing," *Journal of Aircraft*, vol. 25, pp. 236-243, 1988.

5. Wood N. and Nielsen J., "Circulation Control Airfoils-Past, Present, Future." AIAA Paper 85-0204, 23rd Aerospace Sciences Meeting, Reno, Nevada, January 14-17, 1985.

6. Englar R. J., Trobaugh L. A., and Hemmersly R., "STOL Potential of the Circulation Control Wing for High-Performance Aircraft," *Journal of Aircraft*, vol. 14, pp. 175-181, 1978.

7. Englar R. J., "Circulation Control for High Lift and Drag Generation on STOL Aircraft," *Journal of Aircraft*, vol. 12, pp. 457-463, 1975.

8. Wygnanski I., "The Variables Affecting The Control Separation by Periodic Excitation." AIAA 2004-2625, AIAA Fluid Dynamics Conference, Portland Oregon, June 2004.

9. McManus K. and Magill J., "Airfoil Performance Enhancement Using Pulsed Jet Separation Control." AIAA Paper 1997-1971, 4th Shear Flow Control Conference, Snowmass Village, Colorado, June 29-July 2, 1997.

10. Johari H. and McManus K., "Visualization of Pulsed Vortex Generator Jets for Active Control of Boundary Layer Separation." AIAA Paper 1997-2021, 28th Fluid Dynamic Conference, Snowmass Village, Colorado, June 29-July 2, 1997.

11. Smith A., "High-Lift Aerodynamics," *Journal of Aircraft*, vol. 12, pp. 501-530, 1975.

12. Lin J., Robinson S., McGhee R., and Valarezo W., "Separation Control on High Reynolds Number Multi-Element Airfoils." AIAA Paper 92-2636, 10th Applied Aerodynamics Conference, Palo Alto, California, June 22-14, 1992.

13. Zha, G.-C., Carroll, B., Paxton, C., Conley, C., Wells, A., "High Performance Airfoil Using Co-Flow Jet Flow Control." AIAA Paper 2005-1260, 43rd Aerospace Sciences Meeting, Reno, Nevada, January 10-13, 2005.

14. Griffin, B., "Three-Component Wind-Tunnel Balance." B.S. Thesis, University of Florida, 2003.

15. Holman, J., Experimental Methods for Engineers. Seventh Edition. New York: McGraw-Hill, 2001: 100.

BIOGRAPHICAL SKETCH

Adam Joseph Wells was born on July 7, 1979, in Kankakee, IL. After graduating Herscher High School in 1997, he attended Kankakee Community College (KCC) where he earned an associate degree in engineering science in 2000. Adam worked full time at Cognis Corporation during his studies at KCC. Because of the job, he wanted to continue his education at a school within commuting distance from Kankakee. Purdue University Calumet (PUC) was the school that was chosen. Adam attended PUC for one year studying mechanical engineering. At this time, the Cognis Corporation started to down size and have voluntary layoffs. Adam took this opportunity to change his educational focus to aerospace engineering and move to Florida. Adam earned his bachelor's degree in aerospace engineering at the University of Florida in 2003 graduating cum laude. He continued his education at the University of Florida where he earned his Master of Science degree in aerospace engineering in 2005.